

RESEARCH ARTICLE

The complete cell lineage and MAPK- and Otx-dependent specification of the dopaminergic cells in the *Ciona* brain

Kouhei Oonuma* and Takehiro G. Kusakabe

ABSTRACT

The *Ciona* larva has served as a unique model for understanding the development of dopaminergic cells at single-cell resolution owing to the exceptionally small number of neurons in its brain and its fixed cell lineage during embryogenesis. A recent study suggested that the transcription factors *Fer2* and *Meis* directly regulate the dopamine synthesis genes in *Ciona*, but the dopaminergic cell lineage and the gene regulatory networks that control the development of dopaminergic cells have not been fully elucidated. Here, we reveal that the dopaminergic cells in *Ciona* are derived from a bilateral pair of cells called a9.37 cells at the center of the neural plate. The a9.37 cells divide along the anterior-posterior axis, and all of the descendants of the posterior daughter cells differentiate into the dopaminergic cells. We show that the MAPK pathway and the transcription factor *Otx* are required for the expression of *Fer2* in the dopaminergic cell lineage. Our findings establish the cellular and molecular framework for fully understanding the commitment to dopaminergic cells in the simple chordate brain.

KEY WORDS: Brain, Cell lineage, Dopaminergic cell, MAPK pathway, *Otx*, *Ciona*

INTRODUCTION

Dopamine (DA) is a neurotransmitter that is crucial for the regulation of animal behaviors such as mating, feeding and other motivated behaviors, and in humans DA is related to neurological diseases, including Parkinson disease, schizophrenia, multiple sclerosis, attention deficit hyperactivity disorder (ADHD), and Tourette syndrome (Klein et al., 2019; Montarolo et al., 2019; Paschou et al., 2013). Studies of the developmental mechanisms of dopaminergic cells (DA cells) will thus contribute to a better understanding of brain development as well as therapeutics for neurological disorders.

Vertebrates have several classes of DA cells in the brain. For example, the mammalian brain contains DA nuclei in the mesencephalon (A8-A10 DA nuclei), the diencephalon (A11-A15, A17 DA nuclei) and the olfactory bulb in the telencephalon (A16 DA nuclei) (Arenas et al., 2015; Yamamoto and Vernier, 2011). Secreted factors and *trans*-acting factors that are crucial for the development of DA cells have been reported. In the mesencephalon of vertebrates, secreted factors, such as FGF, Shh and Wnt, regulate transcription factors that control the expression of genes related

to DA synthesis (DA pathway genes) (Arenas et al., 2015; Flames and Hobert, 2011; Yamamoto and Vernier, 2011). Factors that are important for the development of DA cells in regions other than the mesencephalon are also well known (Flames and Hobert, 2011; Yamamoto and Vernier, 2011). However, those factors are expressed not only in some DA nuclei but also in neuron subtypes other than DA cells. The regulatory mechanisms that specifically generate DA cells in individual DA nuclei are not yet understood.


The *Ciona* larva has served as a unique model for the study of the development of DA cells in chordate brains (Horie et al., 2018; Moret et al., 2005a; Razy-Krajka et al., 2012). The central nervous system of the *Ciona* larva consists of only a few hundred cells, of which approximately 180 are neurons (Ryan et al., 2016). Ascidian embryos have a fixed cell lineage (Conklin, 1905; Guignard et al., 2020; Nicol and Meinertzhagen, 1988a,b; Nishida, 1987). In ascidian larvae, a single cluster of cells extends a coronet-like protrusion to the cavity of the brain vesicle (Dilly, 1969; Eakin and Kuda, 1971; Konno et al., 2010; Moret et al., 2005a; Nicol and Meinertzhagen, 1991; Ryan et al., 2016; Taniguchi and Nishida, 2004), and most (if not all) of these cells have been considered to be DA cells in the *Ciona* larva (Moret et al., 2005a; Razy-Krajka et al., 2012; Ryan et al., 2016). The coronet-like structure evokes the coronet cells of the saccus vasculosus in the hypothalamus of the fish brain, and it has been proposed that the DA cells of the ascidian larva are homologous to the coronet cells of fish (Moret et al., 2005a; Razy-Krajka et al., 2012). The *Ciona* larva thus enables us to examine the development of the DA cells resembling the saccus vasculosus of the hypothalamus of fish at single-cell resolution, from the stage of the fertilized egg.

It was recently shown that two transcription factors, *Fer2* (previously described as *Ptf1a/PTFb*; see Gyoja and Satoh, 2013 for the orthologous families of the bHLH transcription factors) and *Meis*, directly regulate the expression of DA pathway genes, such as *Tyrosine hydroxylase* (*Th*) (Horie et al., 2018). However, the developmental commitment of DA cells and the relevant regulatory mechanisms remain poorly understood owing to a lack of information about the DA cell lineage. Determination of the precise cell lineage for the *Ciona* brain has been difficult because removal of the chorion, which is a commonly used experimental method for embryonic manipulation in *Ciona*, disrupts both the structure and the left-right asymmetry of the brain vesicle during *Ciona* embryogenesis (Oonuma et al., 2016; Shimeld and Levin, 2006). Previously, we overcame this difficulty by using a combination of new methods that allowed us to analyze the cell lineage in embryos with an intact chorion; with these methods, we determined the precise cell lineage of the *Ciona* brain photoreceptor cells (Oonuma et al., 2016; Oonuma and Kusakabe, 2019).

In the present study, we applied our lineage determination strategy to DA cells in the *Ciona* larva. Our results revealed that a bilateral pair of medial neural plate cells gives rise to all DA cells. A rotatory movement of brain vesicle cells seems to localize DA cells

Institute for Integrative Neurobiology and Department of Biology, Faculty of Science and Engineering, Konan University, Kobe 658-8501, Japan.

*Author for correspondence (kouhei.oonuma@gmail.com)

 K.O., 0000-0002-2418-0865; T.G.K., 0000-0002-8325-3665

Handling Editor: François Guillemot

Received 17 November 2020; Accepted 17 May 2021

to the left wall of the larval brain. The clarification of the precise cell lineage at single-cell resolution allowed us to identify the MAPK pathway and the transcription factor Otx as molecular components that specify the DA cell fate. Our findings thus reveal the complete DA cell lineage, DA specification factors, and the timing of commitment to the DA cell lineage. This study is an important step towards a full understanding of the development of DA cells at the single-cell level.

RESULTS

Dopaminergic cells are derived from a bilateral pair of a-lineage cells of the neural plate

To elucidate the cell lineage of DA cells in *Ciona*, we labeled cells of interest in the neural plate using the photoconvertible fluorescent protein Kaede and then detected expression of the enhanced green

fluorescent protein (EGFP) variant G-GECO1.1, driven by the *cis*-regulatory region of the DA cell-specific gene *Fer2*, at the larval stage. Hereafter, we refer to G-GECO1.1 as EGFPv. The brain vesicle of the ascidian larva is derived from 18 neural plate cells, including a- and A-lineage cells (Fig. 1A). We first examined whether A-lineage cells develop to DA cells by introducing two DNA constructs, *FoxB*>Kaede-NLS and *Fer2*>EGFPv, into the fertilized eggs with the chorion. When each pair of A-lineage cells in the neural plate, i.e. A9.14/A9.14, A9.16/A9.16 and A9.13/A9.13 (right cells underlined), was labeled with photoconverted Kaede, EGFPv was not detected in the labeled A-lineage cells at the larval stage (Fig. 1D-I''; Movies 1-3). This result showed that the A-lineage cells did not give rise to DA cells. We then investigated whether DA cells are derived from a-lineage cells by introducing *Dmrt1*>Kaede-NLS and *Fer2*>EGFPv. When rows III and IV of the

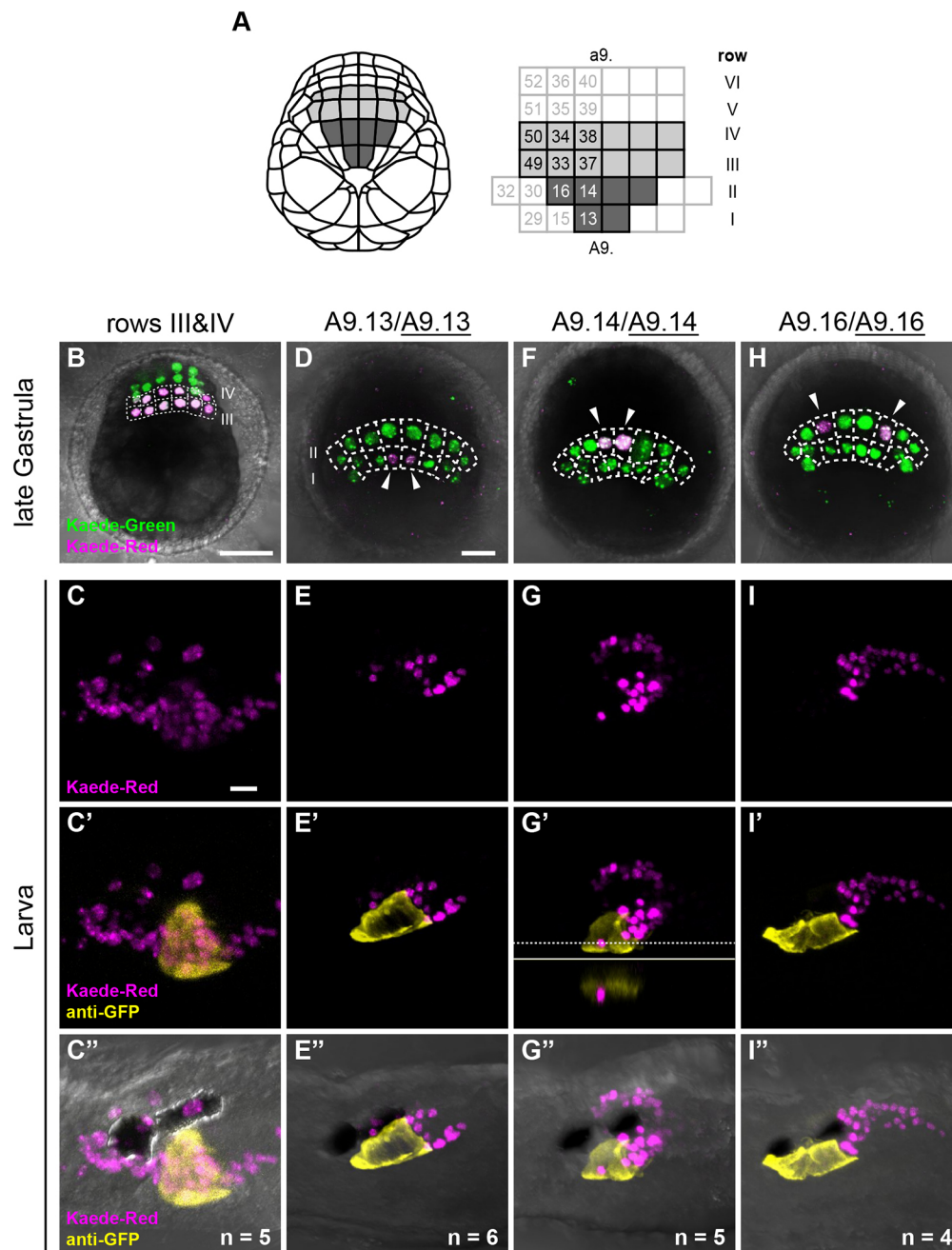


Fig. 1. Dopaminergic cells in *Ciona* are derived from a-lineage cells but not A-lineage cells. (A) Schematic of the late gastrula embryo and the neural plate cells that give rise to the brain vesicle of the *Ciona* larva. Left: Dorsal view of a whole embryo. Anterior is to the top. Right: Six rows (rows I-VI) of neural plate cells. The brain-lineage cells and the non-brain cells are surrounded by black lines and gray lines, respectively. Cells of the brain vesicle of the larva are derived from a-lineage cells (light gray) and A-lineage cells (dark gray). (B-I'') Results of the developmental fate analysis of a-lineage cells and A-lineage cells of the neural plate. (B, D, F, H) Kaede-NLS was expressed in a-lineage cells (rows III and IV) using the promoter/enhancer region of the *Dmrt1* gene (B) and in A-lineage cells (rows I and II) using the *cis*-regulatory region of *FoxB* (D, F, H). Anterior is to the top. Dorsal views. Unconverted Kaede (green) and photo-converted Kaede (magenta) fluorescence is shown. Arrowheads indicate cells exhibiting photo-converted Kaede fluorescence. (C-C'', E-E'', G-G'', I-I'') At the larval stage, the distribution of cells labeled with photo-converted Kaede (magenta) was compared with that of DA cells labeled with EGFPv (yellow) expressed under control of the *cis*-regulatory region of *Fer2*. (C'', E'', G'', I'') Brightfield images merged with fluorescence images. Anterior is to the left. Lateral views. In the lower panel of G', the reconstructed section at the position indicated by the horizontal line in the upper panel shows that the photo-converted cell does not overlap with the DA cells. Scale bars: 10 μm.

neural plate were labeled with photo-converted Kaede, the labeled cells expressed EGFPv at the larval stage (Fig. 1B-C"). Therefore, DA cells are derived from a-lineage cells but not A-lineage cells.

To determine the DA cell lineage further, we labeled each pair of both left and right cells in the a-lineage of the neural plate, namely, the a9.37/a9.37 pair, the a9.38/a9.38 pair, the a9.33/a9.33 pair, the a9.34/a9.34 pair, the a9.49/a9.49 pair and the a9.50/a9.50 pair. Photo-converted Kaede fluorescence was detected in DA cells only when the a9.37/a9.37 pair was labeled, not the other a-lineage cells (Fig. 2; Movies 4-9). Next, we examined whether DA cells are derived equally from the left and right a9.37 cells by labeling either the left a9.37 cell or the right a9.37 cell alone with photo-converted Kaede in the embryos carrying *Dmrt1*>Kaede-NLS and *Fer2*>EGFPv. The number of the cells co-labeled with Kaede-red and EGFPv was about the same between the left a9.37-labeled embryos and the right a9.37-labeled embryos (Fig. 3A,B,B",C,D,D"; Table S1; Movies 10 and 11). In these embryos, the number of the EGFPv-positive cells labeled with Kaede-green but not Kaede-red was similar to the number of the EGFPv-positive cells labeled with Kaede-red (Fig. 3B',B",D',D"; Table S1). These results suggest that the left and right a9.37 cells give rise to DA cells to an equal degree.

Spatial distribution of the descendants of the neural plate cells

In the experiments described above, we also examined the spatial distribution patterns of the descendants of each neural plate cell in the brain vesicle. Overall, there was little position variation of the labeled cells among individuals (Fig. S1). When both a9.37/a9.37

cells (which were bilaterally located along the midline) were labeled, approximately 24 labeled descendants were observed, and these were located at the left-ventral region of the brain vesicle (Fig. 2G-G"; Table S2). When either a left or right a9.37 cell alone was labeled, the right-cell descendants tended to be located at the anterior region, and the left-cell descendants tended to be located at the posterior region in the DA cell population (Fig. 3A-D"). These results suggested that the descendants of the a9.37 cells rotate in a counterclockwise direction when viewed from the dorsal side during the embryogenesis.

To confirm the rotation in the a9.37-lineage cells, we labeled the left or the right side of the embryos by introducing fluorescein isothiocyanate (FITC) dye at the two-cell stage, and we detected the expression of *Fer2* as a marker of a9.37-lineage cells. At 13 h post-fertilization (hpf), cells expressing *Fer2* were located left-right symmetrically (Fig. 3E-F"). By contrast, the boundary between the left- and right-derived descendants of a9.37 cells was slightly tilted counterclockwise at 15 hpf when viewed from the dorsal side of the brain vesicle, and the left-right asymmetry was remarkable at 17 hpf (Fig. 3G-J"). These results revealed that the a9.37-lineage cells rotate counterclockwise when viewed from the dorsal side from 15 hpf or possibly earlier. A similar rotation was also suggested in the descendants of a9.33/a9.33 cells, which included approximately 18 cells, because about half of these cells were located anterior to the DA cells and the other half were located posterior to the DA cells at the larval stage (Fig. 2H-H"; Movie 5; Table S2). To verify the rotation of a9.33-derived cells, we labeled a left and a right a9.33 cell with photoconverted Kaede. The labeled cells derived from the

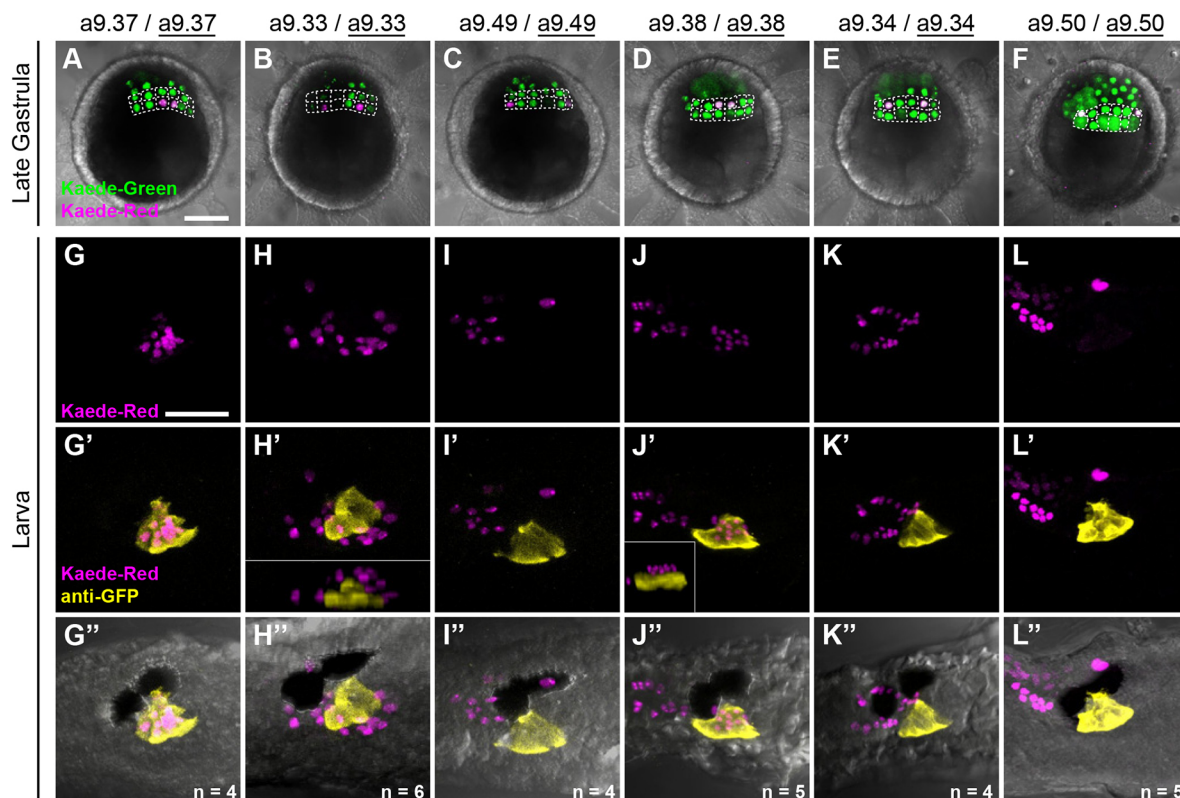


Fig. 2. Left and right a9.37 cells give rise to DA cells. (A-F) Late gastrula embryos in which a particular bilateral pair of a-lineage neural plate cells were labeled with photo-converted Kaede are shown. Anterior is to the top. Dorsal views. White dashed lines delineate rows III and IV of the neural plate. (G-L") At the larval stage, DA cells were visualized by immunofluorescence staining of the GFP reporter (yellow) and compared with photo-converted Kaede (magenta). (G',H',I',J',K',L") Brightfield images merged with fluorescence images. Anterior is to the left. Lateral views. In H' and J', the inset shows the 3D reconstruction demonstrating that the Kaede and EGFPv signals did not overlap each other. Scale bars: 10 μ m.

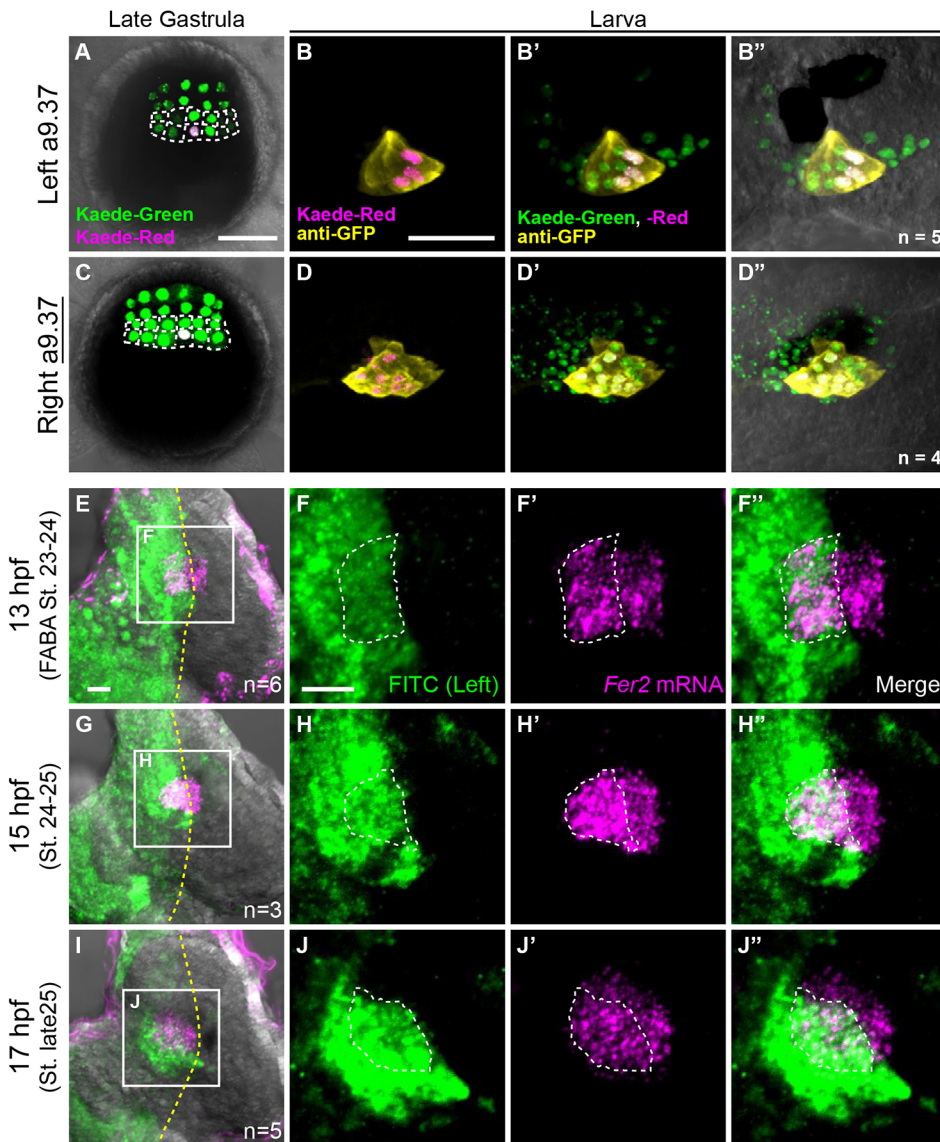


Fig. 3. DA cells are equally derived from left and right a9.37 cells. (A,C) Kaede was photo-converted in either the left a9.37 cell or right a9.37 cell at the late gastrula stage. Anterior is to the top. Dorsal views. White dashed lines delineate the neural plate cells of rows III and IV, which develop into the brain vesicle of the larva. (B-B'',D-D'') Immunofluorescence staining of the GFP reporter (yellow) was performed in larvae expressing the non-converted Kaede (green) and the photo-converted Kaede (magenta). (B'',D'') Brightfield images merged with fluorescence images. Anterior is to the left. Lateral views. (E-J'') Counterclockwise rotation of a9.37-lineage cells in embryos in which the left blastomeres were labeled with FITC. Anterior is to the top. Dorsal views. *Fer2* mRNA (magenta) was detected by WISH. The detection of FITC (green) was performed by immunofluorescent staining before the detection of *Fer2* transcripts. Yellow dashed lines indicate the midline of the embryos. White dashed lines outline the left a9.37-lineage cells. Scale bars: 10 µm.

left a9.33 cell were located posterior to the DA cells at the larval stage, whereas the descendants of the right a9.33 cell (with the exception of a single cell) were located anterior to the DA cells (Fig. S2). Thus, a9.33/a9.33-derived cells also rotate counterclockwise, like the a9.37/a9.37 descendants.

Approximately 24 descendants of the a9.38/a9.38 pair formed two groups with different locations (Table S2). One group was located in the anterior medial and ventral regions of the brain vesicle, and the other group was located dorsally to the DA cells (Fig. 2J-J''). Because the a9.38/a9.38 cells are anterior to the DA progenitor a9.37/a9.37 cells in the *Ciona* neural plate (Fig. 1A), a rearrangement of the relative positions between these cells must occur during brain vesicle development; namely, the a9.37/a9.37-lineage cells move ventrally to the a9.38/a9.38-lineage cells, or the a9.38/a9.38 descendants move to the dorsal side of the a9.37/a9.37 descendants.

The number of descendants of the a9.34/a9.34, a9.49/a9.49, a9.50/a9.50, A9.13/A9.13, A9.14/A9.14 and A9.16/A9.16 pairs in the brain vesicle were approximately 24, 10, 12, 25, 48 and 48, respectively (Table S2). Most of the descendants of a9.49/a9.49 and a9.50/a9.50 were located at the dorsal side of the anterior brain vesicle (Fig. 2I-I'',L-L''). One or two labeled cells derived from

a9.50/a9.50 cells were located at the dorsal side of the pigmented ocellus, indicating that some descendants of a9.50/a9.50 cells move posteriorly during larval development. The descendants of the a9.34/a9.34 pair surrounded the otolith pigment cell (Fig. 2K-K''). Most of the A9.13/A9.13-lineage cells were located at the region posterior to the DA cells, the neck and the anterior nerve cord (Fig. 1E-E''). Some descendants were observed in the anterior brain vesicle. The descendants of A9.14/A9.14 were located at both the left and right regions of the posterior brain vesicle (Fig. 1G-G''). The right population of the labeled cells was reported to differentiate into photoreceptor cells of the pigmented ocellus (Oonuma et al., 2016). A9.16/A9.16-lineage cells were located at the posterior brain vesicle and the neck region (Fig. 1I-I''), which is consistent with a previous study (Cole and Meinertzhagen, 2004).

The DA cell population comprises 16 cells derived from the posterior daughter cells of a9.37/a9.37

To characterize the complete DA cell lineage, we chased both the left and right a9.37 cells throughout embryogenesis. As a probe to chase the a9.37-lineage, we detected transcripts of the DA cell-specific gene *Fer2* (Horie et al., 2018; Razy-Krajka et al., 2012) by

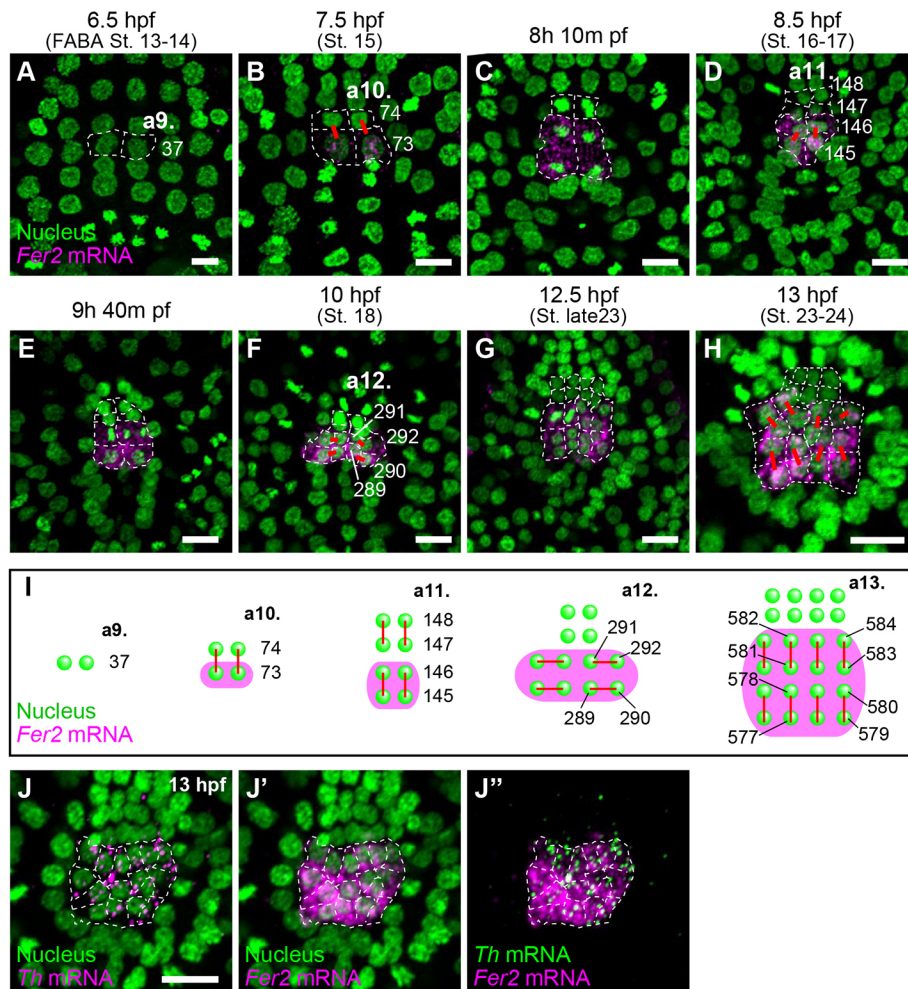


Fig. 4. DA cells are descendants of the posterior daughter cells of a9.37 cells. (A-H) The developmental expression profiles of *Fer2* were examined by fluorescence *in situ* hybridization. *Fer2* transcripts are shown in magenta. Nuclei were counterstained with DAPI (green). Anterior is to the top. Dorsal views. White dashed lines delineate a9.37-lineage cells. Cell division patterns are indicated by red lines connecting sister cells. (I) Schematic of the cell division patterns through development of a9.37-lineage cells. Green: nuclei of a9.37-lineage cells. Magenta: *Fer2* transcripts. Anterior is to the top. Dorsal views. Numbers indicate the standard nomenclature of a9.37-lineage cells. Cell division patterns are indicated by red lines connecting nuclei of sister cells. (J-J'') Both *Fer2* and *Th* were co-expressed in only 16 cells (surrounded by white dashed lines). Nuclei were counterstained with DAPI. Anterior is to the top. Dorsal views. Scale bars: 10 μ m.

whole-mount *in situ* hybridization (WISH). Although *Fer2* mRNA was not detected in the a9.37 cells, the posterior daughter cells (a10.73/a10.73) expressed *Fer2* at 7.5 hpf (Fig. 4A,B,I). The *Fer2*-expressing a10.73 cells divided along the anterior-posterior axis (Fig. 4C,D,I). The 11th generation cells (a11.145/a11.145 and a11.146/a11.146) divided along the left-right axis at 9 h 40 min to 10 hpf and continued to express *Fer2* (Fig. 4E,F,I). The divisions of the eight 12th generation cells along the anterior-posterior axis were observed from 12 h 30 min to 13 hpf (Fig. 4G-I). In the resultant 16 cells, *Fer2* and *Th* were expressed (Fig. 4J-J''), which is consistent with a report suggesting that the expression of *Th* is directly regulated by *Fer2* (Horie et al., 2018). These findings revealed that the number of a9.37-cell descendants expressing *Fer2* becomes 16 by 13 hpf (the late tailbud stage).

Th encodes tyrosine hydroxylase, which generates a precursor of dopamine (L-DOPA) from tyrosine, and is specifically expressed in DA cells. To determine whether the 16 cells expressing both *Fer2* and *Th* at the late tailbud stage differentiate into DA cells, we counted the number of cells expressing *Fer2* and *Th* after 13 hpf (Table 1). At 15 and 17 hpf, *Fer2* mRNA was detected in all 16 cells, indicating that the 16 cells derived from the a10.73/a10.73 cells continuously express *Fer2*. Likewise, *Th* was expressed in approximately 16 cells from pre-hatched embryos (17 hpf) to hatched larvae (18-21 hpf) (Table 1). These results suggest that the total number of DA cells is 16 and that all DA cells are derived from the a10.73/a10.73 pair.

We also examined the expression patterns of the transcription factor *Meis*, which has been suggested to regulate the expression of

Table 1. The average number of cells expressing *Fer2* or *Th*

Stage	Cells expressing <i>Fer2</i>			Cells expressing <i>Th</i>		
		s.e.m.	n		s.e.m.	n
15 hpf	16.00	0.00	3	—	—	—
17 hpf	16.00	0.00	6	16.14	0.14	7
18 hpf	—	—	—	15.89	0.11	9
19 hpf	—	—	—	15.67	0.21	6
21 hpf	—	—	—	15.67	0.24	9

DA marker genes such as *Th* (Horie et al., 2018). In contrast to the DA cell-specific expression of *Fer2*, *Meis* started to be expressed in both a10.73 and a10.74 cells, and the expression continued in the descendants of these cells (Fig. S3A-D''). *Th* expression started in the late a11.145 and a11.146 cells (Fig. S3E-F''). These results are consistent with the suggestion that *Fer2* and *Meis* synergistically regulate the expression of the DA marker genes (Horie et al., 2018).

The MAPK pathway is required for the DA cell fate

We next investigated the molecular mechanisms of the developmental fate decision for DA cells. Our findings revealed that all of the descendants of a10.73 cells expressed the DA cell marker *Th* and appeared to differentiate into DA cells. By contrast, the sister cells, a10.74, and their descendants did not express either *Fer2* or *Th*. Thus, the division of a9.37 cells, giving rise to a10.73 and a10.74 cells, segregates the developmental fate of the DA cells from the non-DA cell fate.

We focused on the FGF/MAPK pathway because this signaling pathway generates the anterior-posterior regionalization of the neural plate in *Ciona* embryos (Hudson, 2016). Indeed, we detected the double phosphorylation of ERK (dpERK), a marker of the MAPK pathway, in the a10.73 cells but not in the a10.74 cells (Fig. S4A-A"). To determine whether FGF/MAPK signaling regulates the developmental fate of the a10.73 cells, we performed pharmacological inhibition of the FGF receptor and MEK, which phosphorylates and activates ERK. Because the treatment with an FGF receptor inhibitor, SU5402, repressed cell division in row III of the neural plate (Fig. S5), we could not examine MAPK pathway activation. In contrast, when embryos were treated with a MEK inhibitor, U0126, from 6.5 hpf, the expression of *Fer2* in the a10.73 cells and their descendants was lost (Fig. 5A-B'; Fig. S6). The MAPK pathway is therefore required for the expression of *Fer2* in the a10.73 cells of the *Ciona* embryo.

In our examination of the *Ciona* Ghost database (Imai et al., 2004), we noted that the *Achaete-Scute a-like1* (*Acsal1*) gene seemed to be expressed in cells anteriorly adjacent to cells expressing *Fer2* at the early tailbud stage. Herein, we confirmed the expression patterns of *Fer2* and *Acsal1* (Fig. S7A,A'). *Acsal1* was expressed in the a10.74 cells, but not in their mother cells, a9.37 cells (Fig. S7B-C"). We thus used *Acsal1* as a specific marker of a10.74 and examined whether the fate of a10.73 cells was transformed into the a10.74-like fate by a MEK inhibitor. When embryos were treated with U0126, *Acsal1* was expressed in the a10.73 cells as well as in the a10.74 cells (Fig. 5C-D'). These results indicate that the MAPK pathway represses the a10.74-like fate in the a10.73 cells and directs them to the DA cell fate.

FGF signaling regulates the regionalization of the neural plate of ascidian embryos via the MAPK pathway, and one of the FGF ligands, *Fgf9/16/20*, was reported to be expressed in cells near a9.37 cells (Hudson and Yasuo, 2005; Hudson et al., 2007). We detected the expression of *Fgf9/16/20* in cells that were anteriorly and posteriorly adjacent to the a9.37 cells and their daughter cells, a10.73 and a10.74 (Fig. S8). Moreover, transcripts of *Fgfr*, the only FGF receptor gene in *Ciona*, were broadly expressed in the neural plate (Fig. S8). Therefore, FGF signaling can occur in both a10.73 and a10.74 cells, whereas the MAPK pathway is active only in the a10.73 cells.

In *Ciona* development, ephrin-Eph signaling has been reported to inhibit FGF/MAPK signaling (Haupaix et al., 2013, 2014; Liu and Satou, 2019; Picco et al., 2007). According to the Ghost database, *Efna.b*, *Eph.a* and *Eph.c* are expressed in the anterior neural plate. In

our present experiments, we detected transcripts of *Efna.b* and *Eph.a* in both a10.74 and a10.73 cells, but the expression levels were higher in the a10.73 cells compared with a10.74 cells (Fig. S8). *Eph.c* mRNA was detected at a very low level in the a10.73 and a10.74 cells (Fig. S8). Therefore, we focused on *Eph.a* receptor and generated a dominant-negative form of *Eph.a* (*dnEph.a*) to determine whether ephrin-Eph signaling inhibits the MAPK pathway in the a10.74 cells. When *dnEph.a* was overexpressed in the whole neural plate using the *Etr1* promoter/enhancer (Shimai and Kusakabe, 2018), dpERK was not detected in a10.74 cells, but the signal intensity of dpERK in other cells was higher in embryos overexpressing *dnEph.a* than in control embryos (Fig. S4B,C). These results suggest that ephrin-Eph signaling does not inhibit the MAPK pathway in 10.74 cells.

Otx promotes *Fer2* expression independently of the MAPK pathway

The transcription factor Otx is essential for the development of the anterior central nervous system in animals (Acampora et al., 1995; Foucher et al., 2006; Matsuo et al., 1995; Wada et al., 2004). Otx has been reported to regulate the specification and differentiation of DA cells in mouse (Arenas et al., 2015; Omodei et al., 2008; Panman et al., 2014). Because *Ciona* Otx is continuously expressed in the cell lineage of the brain vesicle, including DA cells from cleavage to the tailbud stages (Hudson and Lemaire, 2001), it is possible that Otx contributes to the development of DA cells by regulating *Fer2* expression and activating the MAPK pathway.

To examine this hypothesis, we knocked down Otx function using an antisense morpholino oligonucleotide (MO). *Fer2* mRNA was detected in control embryos, but not in the Otx morphant embryos (Fig. 6A,B). In contrast to the *Fer2* expression, the presence of dpERK in a10.73 cells was not influenced by Otx MO (Fig. 6C,D). Inhibition of MEK activity by treatment with U0126 also did not affect Otx expression in the mother cells of a10.73 and a10.74 cells, a9.37 cells (Fig. 6E,F). These results suggest that Otx upregulates the expression of *Fer2* and contributes to the specification of the DA cell fate in parallel with the MAPK pathway in a10.73 cells (Fig. 6G).

Outlining putative cell boundaries based on dpERK cytoplasmic signals revealed that a10.73 cells were larger than a10.74 cells in control embryos (Fig. 6C). Consistent with this, a10.73 cell volume was larger than that of a10.74 cells (Fig. S9). In contrast, no difference between a10.73 and a10.74 cell size was observed in the

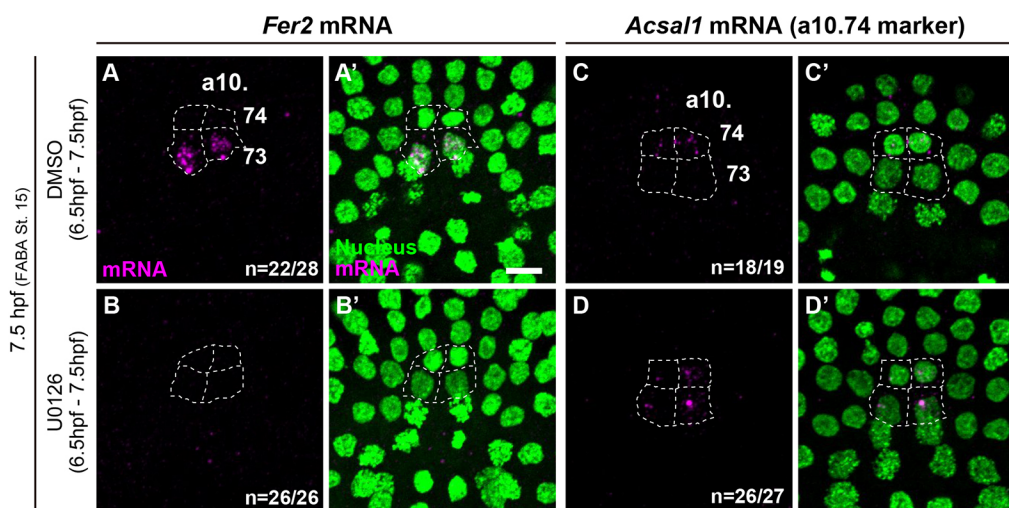


Fig. 5. The MAPK pathway specifies the DA cell fate in a10.73 cells. (A-D') Transcripts of *Fer2* (A-B') and of the a10.74 cell marker gene *Acsal1* (C-D') were detected in embryos treated with DMSO (A,A',C,C') or U0126 (B,B',D,D') by fluorescent WISH. Magenta: expression of *Fer2* and *Acsal1*. Green: nuclei counterstained with DAPI. Anterior is to the top. Dorsal views. White dashed lines delineate a10.73 and a10.74 cells. Scale bars: 10 μ m.

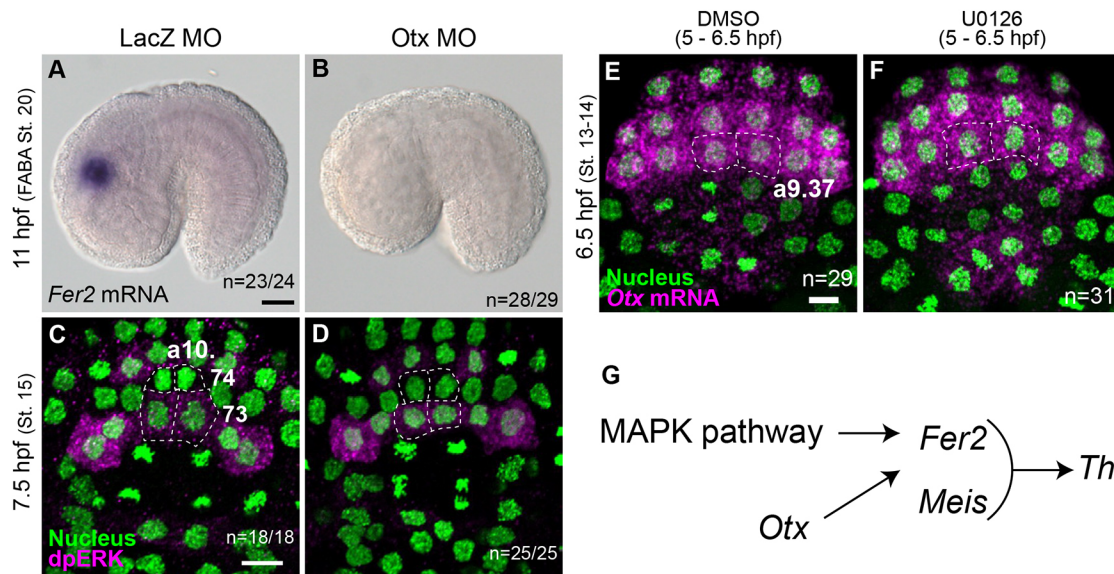


Fig. 6. *Otx* upregulates the expression of *Fer2* independently of the MAPK pathway. (A,B) Expression of *Fer2* in a control embryo (A) and an *Otx* morphant embryo (B) at the early tailbud stage. Anterior is to the left. Lateral view. (C,D) Immunofluorescent staining of dpERK in a control embryo (C) and an *Otx* morphant embryo (D). Anterior is to the top. Dorsal view. (E,F) Expression of *Otx* in a control embryo (E) and an embryo treated with U0126 (F) at the late gastrula stage. Anterior is to the top. Dorsal view. In C-F, the a10.73 and a10.74 cells and their mother cells, a9.37, are indicated by the white dashed lines. (G) Schematic of the gene regulatory networks in DA cell development. *Otx* and the MAPK pathway independently upregulate *Fer2* expression, and then *Fer2* and *Meis* synergistically promote expression of *Th*. Scale bars: 10 μ m.

Otx morphants (Fig. 6D). These findings suggest that there is a difference in cell size between a10.73 and a10.74, which is regulated by *Otx*.

DISCUSSION

We elucidated the complete cell lineage and the number of DA cells in the brain vesicle of the *Ciona* larva. Our results also revealed that the MAPK pathway and *Otx* are essential for the specification of DA cells.

The cell lineage of DA cells

Previous studies have inferred the cell lineage of DA cells in the *Ciona* larva (Cole and Meinertzhagen, 2004; Moret et al., 2005a). Moret et al. (2005a) proposed that DA cells were derived from a9.34/a9.34 or a9.38/a9.38 cells, and Cole and Meinertzhagen (2004) inferred that DA cells were derived from the left a9.33 and a9.37 cells and not from their right counterpart cells. However, the results of these studies were not conclusive, because they were based on observations of unlabeled embryos without the use of DA cell markers (Cole and Meinertzhagen, 2004) or on the expression of marker genes without chasing of cells during their development (Moret et al., 2005a). In this study, by labeling cells of the neural plate and chasing their developmental fates with DA cell markers, we showed that DA cells are derived from both left and right a9.37 cells. We further revealed that all descendants of a10.73 cells, one of the daughter cells of a9.37 cells, develop into DA cells. These findings thus decisively revise the cell lineage of DA cells in the *Ciona* larva. We also revealed that the number of DA cells is 16, which is the same as the number of the coronet cells determined by the previous studies (Ryan et al., 2016; Ryan and Meinertzhagen, 2019). Therefore, it is plausible that all the coronet cells are DA cells. In another ascidian, *Halocynthia roretzi*, it was reported that the coronet cells are derived from the a8.19/a8.19 cells (mother cells of a9.37/a9.37 cells) and the left a8.17 cell (Taniguchi and Nishida, 2004), suggesting a partial conservation of the cell lineage of DA

cells between two ascidian species. In *Halocynthia*, however, only an uncharacterized antigen (Hpr-1) has been used as the coronet cell marker, and other molecular markers, such as *Th* and *Fer2*, have not been identified. Therefore, further investigations are required to understand precisely the species differences of the cell lineage of the DA/coronet cells. The developmental fate of a10.74 cells, the other daughter cells of a9.37 cells, is still unclear. Because two groups of interneurons (cor-ass BVINs and ciliated BVINs) are adjacent to the DA cells (Ryan et al., 2016; Ryan and Meinertzhagen, 2019), a10.74 cells may develop into these interneurons.

With the complete cell lineage of the DA cells in hand, we can now propose the details of the commitment to the DA cell fate at the single-cell level (Fig. 7A). It has been suggested that *Fer2* and *Meis* directly regulate the expression of DA synthesis genes (Horie et al., 2018). The present study revealed that *Fer2* and *Meis* start to be expressed from the early neurula stage in a10.73 cells, all of the descendants of which differentiate to DA cells. The expression of *Th* begins in the daughter cells of a10.73 cells from the initial tailbud stage. These observations suggest that the specification of DA cells occurs in a10.73 cells and then the DA cell fate is determined in their daughter cells, i.e. a11.145 and a11.146 cells (Fig. 7A).

What activates the MAPK pathway only in a10.73 cells?

Our results demonstrated that the MAPK pathway segregates the developmental fate of DA cells between a10.73 and a10.74 cells. The MAPK pathway is active in only a10.73 cells, not in a10.74 cells. What mechanisms are responsible for activating the MAPK pathway exclusively in a10.73 cells? Previous investigations of *Ciona* embryos reported that FGF/MAPK signaling is active in rows I and III of the neural plate, including a9.37 cells (Hudson, 2016; Hudson et al., 2007). A gene encoding the FGF ligand *Fgf9/16/20* is expressed in cells anterior and posterior to the a9.37 cells and their daughter cells, a10.73 and a10.74 (Fig. S8; Haupaix et al., 2014; Hudson, 2016; Hudson and Yasuo, 2005). In contrast to the FGF ligand, a gene encoding the FGF receptor is broadly expressed from

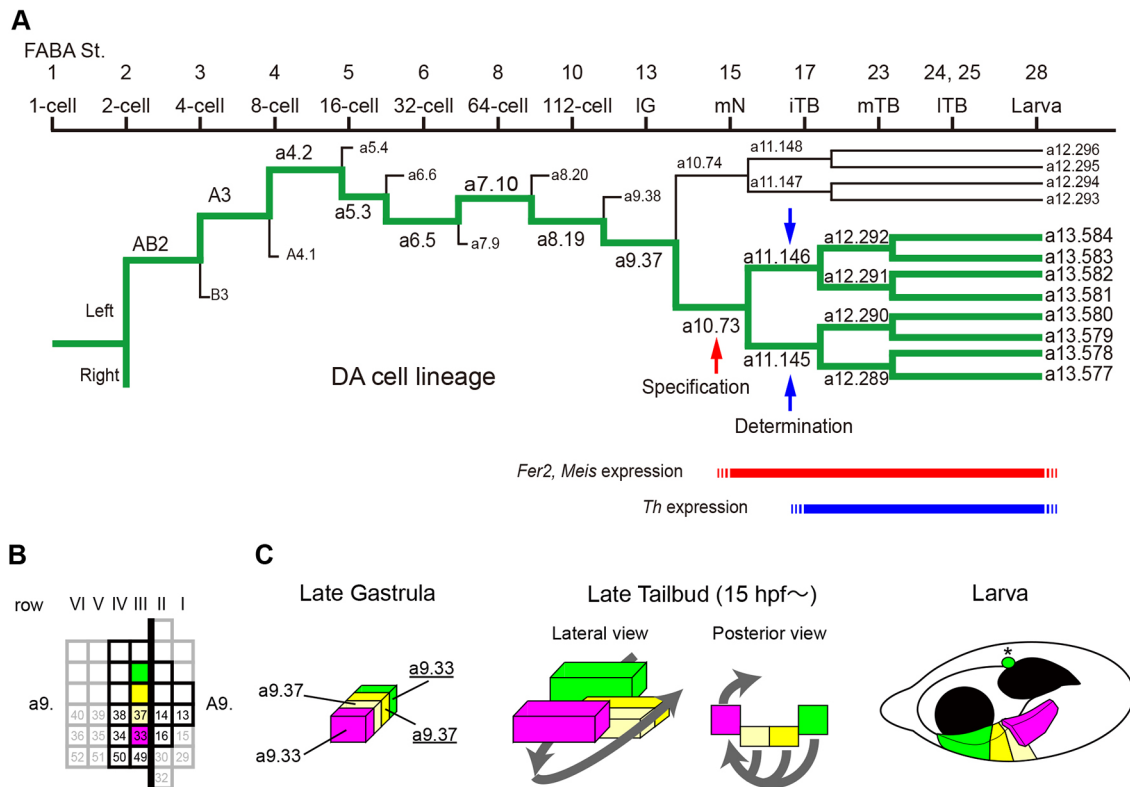


Fig. 7. The *Ciona* DA cell lineage and the developmental movement of neural plate cells. (A) The complete cell lineage of DA cells from the one-cell stage to the larval stage. Only the lineage of the left side is shown. Red and blue bars indicate the period when transcripts of *Fer2/Meis* and *Th* were detected, respectively. Red and blue arrows indicate the times when specification and determination of the DA cell fate occur, respectively. (B) Schematic of the neural plate at the late gastrula stage. Anterior is to the left, and right is to the top. The brain-lineage cells and the non-brain cells are surrounded by black lines and gray lines, respectively. Light yellow: left a9.37; yellow: right a9.37; magenta: left a9.33; green: right a9.33. (C) Schematics of the movement of the descendants of a9.37/a9.37- and a9.33/a9.33 cells. Anterior is to the left, dorsal is to the top. Arrows indicate the movement direction of the a9.37/a9.37- and a9.33/a9.33-lineage cells. Two pigment cells are shown in black. The asterisk indicates an a9.33-derived cell that remains at the right side apart from the other right a9.33-lineage cells. Colors correspond to those used in B.

the late gastrula to the early neurula stages (Fig. S8). We thus speculate that there is competence to respond to FGF in both a10.73 and a10.74 cells, suggesting several possible explanations for the observation of MAPK pathway activation only in a10.73 cells: (1) factors other than the FGF ligand/receptor activate the MAPK pathway in a10.73 cells, (2) the activity of the MAPK pathway derived from the FGF ligand/receptor is inhibited in only a10.74 cells by factors other than ephrin-Eph signaling (Fig. S4B,C), (3) FGF receptor protein in a10.73 cells but not a10.74 cells is preferentially distributed to the side facing the cells expressing the FGF ligand, or (4) the occurrence of FGF/MAPK signaling relies on the ratio of the cell-surface contact with cells providing the FGF ligand (Guignard et al., 2020; Ohta and Satou, 2013; Tassy et al., 2006).

FGF/MAPK signaling induced by FGF8 is required for the development of DA cells in the midbrain of mice and in some regions of the diencephalon of zebrafish (Arenas et al., 2015; Flames and Hobert, 2011; Hegarty et al., 2013; Ryu et al., 2006). The MAPK pathway is thus used for the regulation of the development of DA cells in both *Ciona* and vertebrates.

The role of *Otx* in DA cell development in *Ciona*

We propose two possibilities regarding the role of *Otx* in the development of DA cells in *Ciona*. The first possible mechanism is that *Otx* directly and/or indirectly upregulates the expression of *Fer2* in a10.73 cells in parallel with the MAPK pathway (Fig. 6G). *Otx* is continuously expressed in the DA-lineage cells from cleavage to at

least the tailbud stages, and the transcription regulatory mechanisms of *Otx* change several times during the development (Hudson and Lemaire, 2001; Oonuma et al., 2014). It has been suggested that from the cleavage to the early gastrula stages, *Otx* expression is regulated by the transcription factors GATA and Ets activated by FGF signaling (Bertrand et al., 2003), whereas the transcription factors Sox, Zic and Fox have been suggested to regulate the transcription of *Otx* from the mid to late gastrula stages (Oonuma et al., 2014). Either of these two pathways, i.e. GATA/Ets-*Otx* or Sox/Zic/Fox-*Otx*, may activate *Fer2* in the DA-lineage cells.

The second possible mechanism underlying the role of *Otx* in the development of *Ciona* DA cells is that *Otx* may control the asymmetric cell fate through an unequal cleavage. Interestingly, in *Otx* morphants, the size of a10.74 cells was similar to that of a10.73 cells, whereas in control embryos a10.74 cells were smaller than a10.73 cells (Fig. 6C,D). In ascidians, an unequal cleavage segregates the primordial germ line and somatic cell fates from the 16- to 110-cell stages and this unequal cleavage is related to eccentric positioning of the division plane (Negishi and Nishida, 2017). It is possible that the asymmetric cell size contributes to the distinct fates of a10.73 and a10.74 cells and that *Otx* indirectly controls the unequal cell division via cell division-related factors and/or other factors, such as secreted ligands. Also, because *Fer2* is not expressed in the mother cells of a10.73 cells, i.e. a9.37 cells (in which *Otx* mRNA and dpERK are known to be present), it is possible that there is a repressor that inhibits *Fer2* expression in a9.37 cells and that segregation of this repressor into a10.74 cells is

caused by an unequal cleavage. Given that we observed that treatment with a MEK inhibitor did not influence the size of a10.73 and a10.74 cells, we speculate that the MAPK pathway may not be related to the asymmetric cell size. This speculation is consistent with the parallel regulation of *Fer2* expression by *Otx* and the MAPK pathway.

Our present findings suggest similarities and differences in the developmental mechanisms underlying the development of DA cells between ascidians and vertebrates. In both the brain vesicle of *Ciona* and the midbrain of mammals, the transcription factor *Otx*/*Otx2* is essential for the development of DA cells (Fig. 6A,B; reviewed by Arenas et al., 2015; Flames and Hobert, 2011; Hegarty et al., 2013). In the mouse, *Otx2* has been reported to specify midbrain DA cells via other transcription factors, i.e. *Lmx1a* and *Lmx1b* (Arenas et al., 2015; Flames and Hobert, 2011; Hegarty et al., 2013). Two *Lhx1* genes also regulate the expression of DA marker genes, such as *Th* via *Nurr1/Nr4a2* and *Pitx3*.

In contrast to the mammalian midbrain, the *Otx*-*Fer2*-*Th* pathway is thought to be active in *Ciona*. Because *Lmx1* and *Pitx* homologs of ascidians do not seem to be expressed in the DA-lineage cells (Imai et al., 2004) and given that a *Fer2* homolog does not exist in humans (Gyoja and Satoh, 2013), *Otx* may be the common key factor in DA cell development between ascidians and mammals; in addition, the regulatory factors between *Otx* and the DA pathway genes may have changed during evolution.

Cell movement in the brain vesicle from the tailbud to the larval stages

We chased the labeled cells of the neural plate using Kaede fluorescence in this study. Our results provide new insights into how the brain vesicle of *Ciona* larva develops from the neural plate. We identified three types of cell movement in the brain vesicle. First, the developing brain vesicle rotates clockwise when viewed from the posterior side; as a result, the descendants of both the medial neural plate cells (a9.37/a9.37 and a9.38/a9.38) and the lateral neural plate cells (a9.33/a9.33) become located at the left side of the brain vesicle by the late tailbud stage (Fig. 2G-G", H-H", J-J", Fig. 7B,C). A similar rotation was reported in another ascidian species, *Halocynthia roretzi* (Taniguchi and Nishida, 2004).

Second, descendants of the a9.37/a9.37 and a9.33/a9.33 cells showed counterclockwise rotation when viewed from the dorsal side (Fig. 7C). The movement of the a9.37/a9.37-lineage cells seemed to start from 13 hpf to 15 hpf, because the a9.37/a9.37-lineage cells showed left-right symmetry at 13 hpf but left-right asymmetry at 15 hpf (Fig. 3E-J"). Our findings also revealed that left and right a9.33-lineage cells are located at the posterior and anterior sides of the DA cells, respectively (Fig. S2; Fig. 7C).

Third, the descendants of the posterior neural plate cells a9.37/a9.37 are located ventrally to descendants of the anterior neural plate cells a9.38/a9.38 at the larval stage, suggesting that a rearrangement of these cells occurs in addition to the aforementioned rotations (Fig. 2G-G", J-J"). In these three kinds of the rotations, at least first and second rotations may occur simultaneously because the descendants of a9.37/a9.37 cells tilted counterclockwise and moved to the left side of the brain vesicle during the tailbud stages (Fig. 3E,G,I).

In ascidian larvae, brain vesicle rotation contributes to the generation of left-right asymmetry of the brain vesicle (Ryan et al., 2016; Taniguchi and Nishida, 2004). Vertebrate brains also show left-right asymmetry. For example, the brains of flounder fish exhibit a conspicuous left-right asymmetry that is generated by rotation of the forebrain and left-right asymmetric growth of the

midbrain (Suzuki et al., 2009). The development of the parapineal and pineal gland in fish (Concha and Wilson, 2001; Concha et al., 2012) and the morphology and function of the mammalian brain (Duboc et al., 2015; Kawakami et al., 2008) are other well-known examples of left-right asymmetry in vertebrate brains. These asymmetric brain regions are derived from the forebrain and midbrain. The brain vesicle of the ascidian larva has been considered to be homologous to the forebrain and midbrain of vertebrates (Kusakabe, 2017; Moret et al., 2005b; Wada et al., 1998), although the homology is not fully agreed (e.g. Dufour et al., 2006). The forebrain and midbrain of vertebrates and the brain vesicle of ascidians both function to sense and integrate external information. In both vertebrates and ascidians, Nodal signaling regulates the left-right asymmetry of the brain by influencing the left side (Concha et al., 2012; Kawakami et al., 2008; Nishide et al., 2012; Yoshida and Saiga, 2011). It is thus likely that a common ancestor between ascidians and vertebrates had a left-right asymmetric brain development of which was regulated by Nodal signaling. Left-right asymmetry of sensory information-processing brain regions may have been evolutionarily conserved because of the importance of these regions for brain function.

MATERIALS AND METHODS

Biological materials

Ciona intestinalis type A (also called *C. robusta*) adults were provided by the Maizuru Fisheries Research Station of Kyoto University and by the Misaki Marine Biological Station of the University of Tokyo through the National Bio-Resource Project (NBRP) of the Ministry of Education, Culture, Sports, Science and Technology (MEXT), Japan. Eggs and sperm were obtained surgically from the gonoducts. After insemination, embryos were raised in artificial seawater (Marine Art BR; Tomita Pharmaceutical Company, Tokushima, Japan) containing 0.005% streptomycin sulfate (S6501, Sigma-Aldrich) at 18°C. Embryonic developmental stages were determined according to the FABA Developmental Table (Hotta et al., 2007) and expressed in hpf.

DNA constructs, morpholino oligonucleotides, microinjection and photoconversion

The reporter constructs *Dmrt1*>Kaede-NLS and *FoxB*>Kaede-NLS were generated as described previously (Oonuma et al., 2016). The *Fer2*>G-GECO construct, in which the *cis*-regulatory region of *Fer2* (Horie et al., 2018) is connected with the coding sequence for a GFP-derived Ca²⁺ indicator, G-GECO1.1 (Zhao et al., 2011), was kindly provided by Dr T. Horie (University of Tsukuba, Japan). To construct pSP-*Dmrt1*>PH::GFP, we amplified the open reading frame of PH::GFP from pRN3-PH-GFP, which was a gift from Dr A. McDougall (Université Pierre et Marie Curie and CNRS, France) (forward primer 5'-CCCCTTGCG-GCCGCCATGGACTCGGGCCGGGAC-3'; reverse primer 5'-CAGCTG-GAATTCTTACTTGTACAGCTCGTCCA-3') and a pSP vector containing the *Dmrt1* promoter/enhancer region from *Dmrt1*>Kaede-NLS (forward primer 5'-TAAGAATTCCAGCTGAGCGC-3'; reverse primer 5'-GGC-GGCCGCAAGGGGAT-3') by PCR. Then, these two amplified DNAs were fused using the In-Fusion HD cloning kit (Clontech Laboratories).

To obtain pSP-*Etr*>dn*Eph.a*, we first constructed pSP-*Etr*>Kaede. We amplified the enhancer/promoter region of the *Etr* gene from the *Ciona* genome (forward primer 5'-CTGAAGCTTGCATGCCGACC-ACGGAGTTAATTGA-3'; reverse primer 5'-TCCTCTAGAGTCGAC-TCTGGATAAAGCAATACATACGAG-3') and a pSP-Kaede vector (forward primer 5'-GTCGACTCTAGAGGATCCCC-3'; reverse primer 5'-GCATGCAAGCTTCAGCTG-3') by PCR. Then, we fused these two amplified DNAs using the In-Fusion HD cloning kit (Clontech Laboratories). Next, total RNA was isolated from tailbud embryos at 15 hpf with a NucleoSpin miRNA kit (740971, MACHEREY-NAGEL). First-strand cDNA was prepared from 1.3 µg total RNA with a SuperScript IV First-Strand Synthesis System kit (18091050, Thermo Fisher Scientific),

and used to amplify a cDNA sequence of *Eph.a* by PCR using a pair of primers (forward primer, 5'-CCCCTTGGCGCCGCGCATGGATTATCTGGCTGTCCT-3'; reverse primer, 5'-GCTCAGCTGGAATTCTCACAGTTTAAATCAATTTCTTTCGC-3'). We also amplified a pSP vector containing the upstream region of *Etr* from pSP-*Etr*>Kaede (forward primer 5'-GAATTCAGCTGAGCGCCGGTCG-3'; reverse primer 5'-GGCGGCCGCAAGGGGAT-3') by PCR. Then, these two amplified DNA fragments were fused using the In-Fusion HD cloning kit (Clontech Laboratories).

MOs were obtained from Gene Tools. An antisense MO was arbitrarily designed to bind to the sequence flanking and contain the first methionine codon of the *Otx* gene. As the negative control, an antisense MO against the bacterial *lacZ* gene (Satou et al., 2001) was used. The nucleotide sequences of the MOs were: *Otx*, 5'-TACGACATGTTAGGAATTGAACCCG-3'; *lacZ*, 5'-TACGCTTCTCTTTGGAGCAGTCAT-3' (underlining indicates the complementary sequence of the translation start site). MOs were dissolved at 2 mM in 1 mM Tris-HCl pH 8.0, 0.1 mM EDTA. Wada et al. (2004) reported defects of the adhesive pulp and lack of melanization of the brain pigment cells as the specific phenotype of the *Otx* morphant larvae, and we confirmed the effectiveness of the *Otx* MO by observing this phenotype in all injected larvae ($n=56$).

Microinjection of DNA constructs and MOs into *Ciona* eggs with intact chorion, and photoconversion of Kaede fluorescence were carried out as described previously (Oonuma et al., 2016).

Whole-mount *in situ* hybridization

Whole-mount fluorescent *in situ* hybridization was carried out using digoxigenin- or FITC-labeled RNA probes as described by Oonuma and Kusakabe (2019). To synthesize RNA probes for *Fer2*, *Fgf9/16/20*, *Meis* and *Th*, we used a plasmid clone obtained from the *Ciona* Gene Collection release 1 (Satou et al., 2002): Gene Collection IDs (and KH gene model IDs) R1GC30n10 (*Eph.a*, KH.C1.404), R1GC16p22 (*Eph.c*, KH.C7.568), R1GC21d13 (*Efn.a.b*, KH.C3.202), R1GC44e22 (*Fer2*, previously described as *PTFb/Ptf1a*, KH.L116.39), R1GC29b12 (*Fgf9/16/20*, KH.C2.125), R1GC32j14 (*Fgfr*, KH.S742.2), R1GC32a16 (*Meis*, KH.C10.174), R1CiGC13g19 (*Otx*, KH.C4.84) and R1GC05g24 (*Th*, KH.C2.252). For the synthesis of the RNA probe for *Achaete-Scute a-like1* (*Acsall*, KH.C2.560), the template DNA was obtained as follows. First-strand cDNA from embryos at 15 hpf was used to amplify a cDNA sequence of *Acsall* by PCR using a pair of primers (forward primer, 5'-CGGGGATCCAAACACGTCAACTCTGCG-3'; reverse primer, 5'-TGGGTGCGACCTAATTTATAATTTAGCACTGGTCTTTC-3'; restriction sites are underlined). The amplified sequence was inserted into the BamHI/Sall sites of pBluescript II SK(+). Antisense digoxigenin- and fluorescein-labeled RNA probes were synthesized using T7 RNA polymerase from plasmid DNA linearized with BamHI for *Acsall*, *Efn.a.b*, *Eph.a*, *Eph.c*, *Fer2*, *Fgf9/16/20* and *Meis*, with AclI for *Th* and with Sall for *Eph.a* and *Fgfr*. Recapitulation of the expression patterns of these transcripts was confirmed with at least five embryos.

Immunofluorescent staining

Immunofluorescent staining for G-GECO1.1 and PH::GFP was carried out by the method described by Oonuma et al. (2016). A rabbit anti-GFP antibody (A11122, Thermo Fisher Scientific) was used as the primary antibody (1:1000), and Alexa Fluor 633-conjugated anti-rabbit IgG (A21070, Thermo Fisher Scientific) or Alexa Fluor 488-conjugated anti-rabbit IgG (A11008, Thermo Fisher Scientific) were used as the secondary antibody (1:1000).

Immunofluorescent staining for dpERK was performed as follows. The early neurula embryos (7.5 hpf) with the chorion intact were fixed in 4% paraformaldehyde in 0.1 M MOPS (pH 7.5) and 0.5 M NaCl at room temperature for 30 min and were then washed with T-TBS (Tris-buffered saline, 0.01% Triton X-100). After the embryos were incubated with 80% methanol on ice for 10 min and washed with T-TBS, tungsten needles were used to remove the chorion and then the embryos were incubated in 1% bovine serum albumin (BSA)/T-TBS solution at room temperature for 30 min. The specimens were incubated in signal booster immunostain solution F (BCL-ISF; Beacle) with anti-dpERK mouse IgG antibody

(M9692, Sigma-Aldrich; 1:1000) for 16 h at 4°C. After being washed with T-PBS (0.1% Triton X-100 in PBS), the specimens were incubated in signal booster immunostain solution F with Histofine Simplestain Max-PO(M) (424131, Nichirei Biosciences) as the secondary antibody (1:10) for 2.5 h at room temperature, and then washed three times with T-PBS. Signal amplification was performed with the TSA system using Alexa Fluor 594-conjugated tyramide (T20915, Thermo Fisher Scientific; 1:100) for 20 min at room temperature. Fluorescent images were obtained with a laser scanning confocal microscope (FV1200 IX83, Olympus) at 1-μm intervals in the z-axis.

Pharmacological inhibition

U0126 (U120, Sigma-Aldrich) and SU5402 (SML0443, Sigma-Aldrich) were dissolved at 10 mM in dimethylsulfoxide (DMSO) and stored as stock solution at -25°C. Embryos with intact chorion were treated with 5 μM U0126 or 5 μM SU5402 in artificial sea water from 6.5 to 7.5 hpf.

Cell volume measurement

Membrane-localized GFP was expressed in cells of the neural plate derived from the a-lineage using pSP-*Dmrt1*>PH::GFP, and immunofluorescent staining against GFP was performed. After immunostaining, confocal images of the fluorescent signal were obtained at 1-μm intervals in the z-axis. Then, based on these images, three-dimensional (3D) models of a10.73 and a10.74 cells were constructed using the open source software TrakEM2 that was a plugin of ImageJ (Cardona et al., 2012). From the 3D models, the volume of a10.73 and a10.74 cells was measured using TrakEM2. Statistical analysis was performed using an unpaired Student's *t*-test (two-sided). $P<0.001$ was considered statistically significant.

Acknowledgements

We thank Dr Fuki Gyoja (Konan University) for suggestions and comments on bHLH family classification, Dr Takeo Horie (Tsukuba University) for the *Fer2*>G-GECO DNA construct, and Dr Alex McDougall (Université Pierre et Marie Curie and CNRS) for the pRN3-PH-GFP DNA construct. We also thank Chikako Imaizumi, Reiko Yoshida, Yutaka Satou (Kyoto University), Satoe Aratake, Akihiro Yoshikawa, Megumi Kohtsuka, Manabu Yoshida (The University of Tokyo), and the National BioResource Project (NBRP) of MEXT for providing us with *Ciona* adults.

Competing interests

The authors declare no competing or financial interests.

Author contributions

Conceptualization: K.O., T.G.K.; Methodology: K.O., T.G.K.; Validation: K.O.; Investigation: K.O.; Resources: K.O., T.G.K.; Writing - original draft: K.O., T.G.K.; Writing - review & editing: K.O., T.G.K.; Visualization: K.O.; Supervision: T.G.K.; Project administration: K.O., T.G.K.; Funding acquisition: K.O., T.G.K.

Funding

This study was supported in part by Grants-in-Aid for Scientific Research from the Japan Society for the Promotion of Science (JSPS) to K.O. (17K15130 and 19K16150) and T.G.K. (16H04724 and 19H03213). This study was also supported in part by research grants from the Hirao Taro Foundation of KONAN GAKUEN for Academic Research and the Takeda Science Foundation (2015021209) to T.G.K. and by a Sasakawa Scientific Research Grant from The Japan Science Society to K.O.

Peer review history

The peer review history is available online at <https://journals.biologists.com/dev/article-lookup/doi/10.1242/dev.198754>.

References

- Acampora, D., Mazan, S., Lallemand, Y., Avantaggiato, V., Maury, M., Simeone, A. and Brûlet, P. (1995). Forebrain and midbrain regions are deleted in *Otx2*^{-/-} mutants due to a defective anterior neuroectoderm specification during gastrulation. *Development* **121**, 3279-3290. doi:10.1242/dev.121.10.3279
- Arenas, E., Denham, M. and Villaseca, J. C. (2015). How to make a midbrain dopaminergic neuron. *Development* **142**, 1918-1936. doi:10.1242/dev.097394
- Bertrand, V., Hudson, C., Caillol, D., Popovici, C. and Lemaire, P. (2003). Neural tissue in ascidian embryos is induced by FGF9/16/20, acting via a combination of maternal GATA and Ets transcription factors. *Cell* **115**, 615-627. doi:10.1016/S0092-8674(03)00928-0

- Cardona, A., Saalfeld, S., Schindelin, J., Arganda-Carreras, I., Preibisch, S., Longair, M., Tomancak, P., Hartenstein, V. and Douglas, R. J. (2012). TrakEM2 software for neural circuit reconstruction. *PLoS ONE* **7**, e38011. doi:10.1371/journal.pone.0038011
- Cole, A. G. and Meinertzhagen, I. A. (2004). The central nervous system of the ascidian larva: mitotic history of cells forming the neural tube in late embryonic *Ciona intestinalis*. *Dev. Biol.* **271**, 239–262. doi:10.1016/j.ydbio.2004.04.001
- Concha, M. L. and Wilson, S. W. (2001). Asymmetry in the epithalamus of vertebrates. *J. Anat.* **199**, 63–84. doi:10.1046/j.1469-7580.2001.19910063.x
- Concha, M. L., Bianco, I. H. and Wilson, S. W. (2012). Encoding asymmetry within neural circuits. *Nat. Rev. Neurosci.* **13**, 832–843. doi:10.1038/nrn3371
- Conklin, E. G. (1905). The organization and cell-lineage of the ascidian egg. *J. Acad. Nat. Sci. Phila.* **13**, 1–119. doi:10.5962/bhl.title.4801
- Dilly, P. N. (1969). Studies on the receptors in *Ciona intestinalis*. *Z. Zellforsch. Mikroskop. Anat.* **96**, 63–65. doi:10.1007/BF00321477
- Duboc, V., Dufourcq, P., Blader, P. and Roussigné, M. (2015). Asymmetry of the brain: development and implications. *Annu. Rev. Genet.* **49**, 647–672. doi:10.1146/annurev-genet-112414-055322
- Dufour, H. D., Chettouh, Z., Deyts, C., De Rosa, R., Goriadis, C., Joly, J.-S. and Brunet, J.-F. (2006). Precranial origin of cranial motoneurons. *Proc. Natl. Acad. Sci. USA* **103**, 8727–8732. doi:10.1073/pnas.0600805103
- Eakin, R. M. and Kuda, A. (1971). Ultrastructure of sensory receptors in ascidian tadpoles. *Z. Zellforsch.* **112**, 287–312. doi:10.1007/BF02584045
- Flames, N. and Hobert, O. (2011). Transcriptional control of the terminal fate of monoaminergic neurons. *Annu. Rev. Neurosci.* **34**, 153–184. doi:10.1146/annurev-neuro-061010-113824
- Foucher, I., Mione, M., Simeone, A., Acampora, D., Bally-Cuif, L. and Houart, C. (2006). Differentiation of cerebellar cell identities in absence of Fgf signalling in zebrafish *Otx* morphants. *Development* **133**, 1891–1900. doi:10.1242/dev.02352
- Guignard, L., Fiúza, U.-M., Leggio, B., Laussu, J., Faure, E., Michelin, G., Biasuz, K., Hufnagel, L., Malandain, G., Godin, C. et al. (2020). Contact area-dependent cell communication and the morphological invariance of ascidian embryogenesis. *Science* **369**, eaar5663. doi:10.1126/science.aar5663
- Gyoja, F. and Satoh, N. (2013). Evolutionary aspects of variability in bHLH orthologous families: insights from the pearl oyster, *Pinctada fucata*. *Zoolog. Sci.* **30**, 868–876. doi:10.2108/zsj.30.868
- Haupaix, N., Stolfi, A., Sirour, C., Picco, V., Levine, M., Christiaen, L. and Yasuo, H. (2013). p120RasGAP mediates ephrin/Eph-dependent attenuation of FGF/ERK signals during cell fate specification in ascidian embryos. *Development* **140**, 4347–4352. doi:10.1242/dev.098756
- Haupaix, N., Abitua, P. B., Sirour, C., Yasuo, H., Levine, M. and Hudson, C. (2014). Ephrin-mediated restriction of ERK1/2 activity delimits the number of pigment cells in the *Ciona* CNS. *Dev. Biol.* **394**, 170–180. doi:10.1016/j.ydbio.2014.07.010
- Hegarty, S. V., Sullivan, A. M. and O'keeffe, G. W. (2013). Midbrain dopaminergic neurons: a review of the molecular circuitry that regulates their development. *Dev. Biol.* **379**, 123–138. doi:10.1016/j.ydbio.2013.04.014
- Horie, T., Horie, R., Chen, K., Cao, C., Nakagawa, M., Kusakabe, T. G., Satoh, N., Sasakura, Y. and Levine, M. (2018). Regulatory cocktail for dopaminergic neurons in a protovertebrate identified by whole-embryo single-cell transcriptomics. *Genes Dev.* **32**, 1297–1302. doi:10.1101/gad.317669.118
- Hotta, K., Mitsuhashi, K., Takahashi, H., Inaba, K., Oka, K., Gojobori, T. and Ikeo, K. (2007). A web-based interactive developmental table for the ascidian *Ciona intestinalis*, including 3D real-image embryo reconstructions: I. From fertilized egg to hatching larva. *Dev. Dyn.* **236**, 1790–1805. doi:10.1002/dvdy.21188
- Hudson, C. (2016). The central nervous system of ascidian larvae. *Wiley Interdiscipl. Rev. Dev. Biol.* **5**, 538–561. doi:10.1002/wdev.239
- Hudson, C. and Lemaire, P. (2001). Induction of anterior neural fates in the ascidian *Ciona intestinalis*. *Mech. Dev.* **100**, 189–203. doi:10.1016/S0925-4773(00)00528-1
- Hudson, C. and Yasuo, H. (2005). Patterning across the ascidian neural plate by lateral Nodal signalling sources. *Development* **132**, 1199–1210. doi:10.1242/dev.01688
- Hudson, C., Lotito, S. and Yasuo, H. (2007). Sequential and combinatorial inputs from Nodal, Delta2/Notch and FGF/MEK/ERK signalling pathways establish a grid-like organisation of distinct cell identities in the ascidian neural plate. *Development* **134**, 3527–3537. doi:10.1242/dev.002352
- Imai, K. S., Hino, K., Yagi, K., Satoh, N. and Satou, Y. (2004). Gene expression profiles of transcription factors and signaling molecules in the ascidian embryo: towards a comprehensive understanding of gene networks. *Development* **131**, 4047–4058. doi:10.1242/dev.01270
- Kawakami, R., Dobi, A., Shigemoto, R. and Ito, I. (2008). Right isomerism of the brain in *inversus viscerum* mutant mice. *PLoS ONE* **3**, e1945. doi:10.1371/journal.pone.0001945
- Klein, M. O., Battagello, D. S., Cardoso, A. R., Hauser, D. N., Bittencourt, J. C. and Correa, R. G. (2019). Dopamine: functions, signaling, and association with neurological diseases. *Cell. Mol. Neurobiol.* **39**, 31–59. doi:10.1007/s10571-018-0632-3
- Konno, A., Kaizu, M., Hotta, K., Horie, T., Sasakura, Y., Ikeo, K. and Inaba, K. (2010). Distribution and structural diversity of cilia in tadpole larvae of the ascidian *Ciona intestinalis*. *Dev. Biol.* **337**, 42–62. doi:10.1016/j.ydbio.2009.10.012
- Kusakabe, T. G. (2017). Identifying vertebrate brain prototypes in deuterostomes. In: *Brain Evolution by Design* (ed. S. Shigeno, Y. Murakami and T. Nomura), pp. 153–186. Tokyo: Springer.
- Liu, B. and Satou, Y. (2019). *Foxg* specifies sensory neurons in the anterior neural plate border of the ascidian embryo. *Nat. Commun.* **10**, 4911. doi:10.1038/s41467-019-12839-6
- Matsuo, I., Kuratani, S., Kimura, C., Takeda, N. and Aizawa, S. (1995). Mouse *Otx2* functions in the formation and patterning of rostral head. *Genes Dev.* **9**, 2646–2658. doi:10.1101/gad.9.21.2646
- Montarolo, F., Martire, S., Perga, S. and Bertolotto, A. (2019). NURR1 impairment in multiple sclerosis. *Int. J. Mol. Sci.* **20**, 4858. doi:10.3390/ijms20194858
- Moret, F., Christiaen, L., Deyts, C., Blin, M., Joly, J.-S. and Vernier, P. (2005a). The dopamine-synthesizing cells in the swimming larva of the tunicate *Ciona intestinalis* are located only in the hypothalamus-related domain of the sensory vesicle. *Eur. J. Neurosci.* **21**, 3043–3055. doi:10.1111/j.1460-9568.2005.04147.x
- Moret, F., Christiaen, L., Deyts, C., Blin, M., Vernier, P. and Joly, J.-S. (2005b). Regulatory gene expressions in the ascidian ventral sensory vesicle: evolutionary relationships with the vertebrate hypothalamus. *Dev. Biol.* **277**, 567–579. doi:10.1016/j.ydbio.2004.11.004
- Negishi, T. and Nishida, H. (2017). Asymmetric and unequal cell divisions in ascidian embryos. *Results Probl. Cell Differ.* **61**, 261–284. doi:10.1007/978-3-319-53150-2_12
- Nicol, D. and Meinertzhagen, I. A. (1988a). Development of the central nervous system of the larva of the ascidian, *Ciona intestinalis* L.: I. The early lineages of the neural plate. *Dev. Biol.* **130**, 721–736. doi:10.1016/0012-1606(88)90363-6
- Nicol, D. and Meinertzhagen, I. A. (1988b). Development of the central nervous system of the larva of the ascidian, *Ciona intestinalis* L.: II. Neural plate morphogenesis and cell lineages during neurulation. *Dev. Biol.* **130**, 737–766. doi:10.1016/0012-1606(88)90364-8
- Nicol, D. and Meinertzhagen, I. A. (1991). Cell counts and maps in the larval central nervous system of the ascidian *Ciona intestinalis* (L.). *J. Comp. Neurol.* **309**, 415–429. doi:10.1002/cne.903090402
- Nishida, H. (1987). Cell lineage analysis in ascidian embryos by intracellular injection of a tracer enzyme: III. Up to the tissue restricted stage. *Dev. Biol.* **121**, 526–541. doi:10.1016/0012-1606(87)90188-6
- Nishide, K., Mugitani, M., Kumano, G. and Nishida, H. (2012). Neurula rotation determines left-right asymmetry in ascidian tadpole larvae. *Development* **139**, 1467–1475. doi:10.1242/dev.076083
- Ohta, N. and Satou, Y. (2013). Multiple signaling pathways coordinate to induce a threshold response in a chordate embryo. *PLoS Genet.* **9**, e1003818. doi:10.1371/journal.pgen.1003818
- Omodei, D., Acampora, D., Mancuso, P., Prakash, N., Di Giovannantonio, L. G., Wurst, W. and Simeone, A. (2008). Anterior-posterior graded response to *Otx2* controls proliferation and differentiation of dopaminergic progenitors in the ventral mesencephalon. *Development* **135**, 3459–3470. doi:10.1242/dev.027003
- Oonuma, K. and Kusakabe, T. G. (2019). Spatio-temporal regulation of Rx and mitotic patterns shape the eye-cup of the photoreceptor cells in *Ciona*. *Dev. Biol.* **445**, 245–255. doi:10.1016/j.ydbio.2018.11.011
- Oonuma, K., Hirose, D., Takatori, N. and Saiga, H. (2014). Analysis of the transcription regulatory mechanism of *Otx* during the development of the sensory vesicle in *Ciona intestinalis*. *Zoolog. Sci.* **31**, 565–572. doi:10.2108/zs140060
- Oonuma, K., Tanaka, M., Nishitsuji, K., Kato, Y., Shimai, K. and Kusakabe, T. G. (2016). Revised lineage of larval photoreceptor cells in *Ciona* reveals archetypal collaboration between neural tube and neural crest in sensory organ formation. *Dev. Biol.* **420**, 178–185. doi:10.1016/j.ydbio.2016.10.014
- Panman, L., Papathanou, M., Laguna, A., Oosterveen, T., Volakakis, N., Acampora, D., Kurtsdotter, I., Yoshitake, T., Kehr, J., Joodmardi, E. et al. (2014). *Sox6* and *Otx2* control the specification of substantia nigra and ventral tegmental area dopamine neurons. *Cell Rep.* **8**, 1018–1025. doi:10.1016/j.celrep.2014.07.016
- Paschou, P., Fernandez, T. V., Sharp, F., Heiman, G. A. and Hoekstra, P. J. (2013). Genetic susceptibility and neurotransmitters in Tourette syndrome. *Int. Rev. Neurobiol.* **112**, 155–177. doi:10.1016/B978-0-12-411546-0.00006-8
- Picco, V., Hudson, C. and Yasuo, H. (2007). Ephrin-Eph signalling drives the asymmetric division of notochord/neural precursors in *Ciona* embryos. *Development* **134**, 1491–1497. doi:10.1242/dev.003939
- Razy-Krajka, F., Brown, E. R., Horie, T., Callebort, J., Sasakura, Y., Joly, J.-S., Kusakabe, T. G. and Vernier, P. (2012). Monoaminergic modulation of photoreception in ascidian: evidence for a proto-hypothalamo-retinal territory. *BMC Biol.* **10**, 45. doi:10.1186/1741-7007-10-45
- Ryan, K. and Meinertzhagen, I. A. (2019). Neuronal identity: the neuron types of a simple chordate sibling, the tadpole larva of *Ciona intestinalis*. *Curr. Opin. Neurobiol.* **56**, 47–60. doi:10.1016/j.conb.2018.10.015
- Ryan, K., Lu, Z. and Meinertzhagen, I. A. (2016). The CNS connectome of a tadpole larva of *Ciona intestinalis* (L.) highlights sidedness in the brain of a chordate sibling. *eLife* **5**, e16962. doi:10.7554/eLife.16962

- Ryu, S., Holzschuh, J., Mahler, J. and Driever, W. (2006). Genetic analysis of dopaminergic system development in zebrafish. *J. Neural. Transm.* **70**, 61-66. doi:10.1007/978-3-211-45295-0_11
- Satou, Y., Imai, K. S. and Satoh, N. (2001). Action of morpholinos in *Ciona* embryos. *Genesis* **30**, 103-106. doi:10.1002/gene.1040
- Satou, Y., Yamada, L., Mochizuki, Y., Takatori, N., Kawashima, T., Sasaki, A., Hamaguchi, M., Awazu, S., Yagi, K., Sasakura, Y. et al. (2002). A cDNA resource from the basal chordate *Ciona intestinalis*. *Genesis* **33**, 153-154. doi:10.1002/gene.10119
- Shimai, K. and Kusakabe, T. G. (2018). The use of *cis*-regulatory DNAs as molecular tools. In *Transgenic Ascidians* (ed. Y. Sasakura), pp. 49-68. Singapore: Springer.
- Shimeld, S. M. and Levin, M. (2006). Evidence for the regulation of left-right asymmetry in *Ciona intestinalis* by ion flux. *Dev. Dyn.* **235**, 1543-1553. doi:10.1002/dvdy.20792
- Suzuki, T., Washio, Y., Aritaki, M., Fujinami, Y., Shimizu, D., Uji, S. and Hashimoto, H. (2009). Metamorphic *pitx2* expression in the left habenula correlated with lateralization of eye-sidedness in flounder. *Dev. Growth Differ.* **51**, 797-808. doi:10.1111/j.1440-169X.2009.01139.x
- Taniguchi, K. and Nishida, H. (2004). Tracing cell fate in brain formation during embryogenesis of the ascidian *Halocynthia roretzi*. *Dev. Growth Differ.* **46**, 163-180. doi:10.1111/j.1440-169X.2004.00736.x
- Tassy, O., Daian, F., Hudson, C., Bertrand, V. and Lemaire, P. (2006). A quantitative approach to the study of cell shapes and interactions during early chordate embryogenesis. *Curr. Biol.* **16**, 345-358. doi:10.1016/j.cub.2005.12.044
- Wada, H., Saiga, H., Satoh, N. and Holland, P. W. (1998). Tripartite organization of the ancestral chordate brain and the antiquity of placodes: insights from ascidian *Pax-2/5/8*, *Hox* and *Otx* genes. *Development* **125**, 1113-1122. doi:10.1242/dev.125.6.1113
- Wada, S., Sudou, N. and Saiga, H. (2004). Roles of *Hroth*, the ascidian *otx* gene, in the differentiation of the brain (sensory vesicle) and anterior trunk epidermis in the larval development of *Halocynthia roretzi*. *Mech. Dev.* **121**, 463-474. doi:10.1016/j.mod.2004.03.017
- Yamamoto, K. and Vernier, P. (2011). The evolution of dopamine systems in chordates. *Front. Neuroanat.* **5**, 21. doi:10.3389/fnana.2011.00021
- Yoshida, K. and Saiga, H. (2011). Repression of *Rx* gene on the left side of the sensory vesicle by Nodal signaling is crucial for right-sided formation of the ocellus photoreceptor in the development of *Ciona intestinalis*. *Dev. Biol.* **354**, 144-150. doi:10.1016/j.ydbio.2011.03.006
- Zhao, Y., Araki, S., Wu, J., Teramoto, T., Chang, Y.-F., Nakano, M., Abdelfattah, A. S., Fujiwara, M., Ishihara, T., Nagai, T. et al. (2011). An expanded palette of genetically encoded Ca^{2+} indicators. *Science* **333**, 1888-1891. doi:10.1126/science.1208592

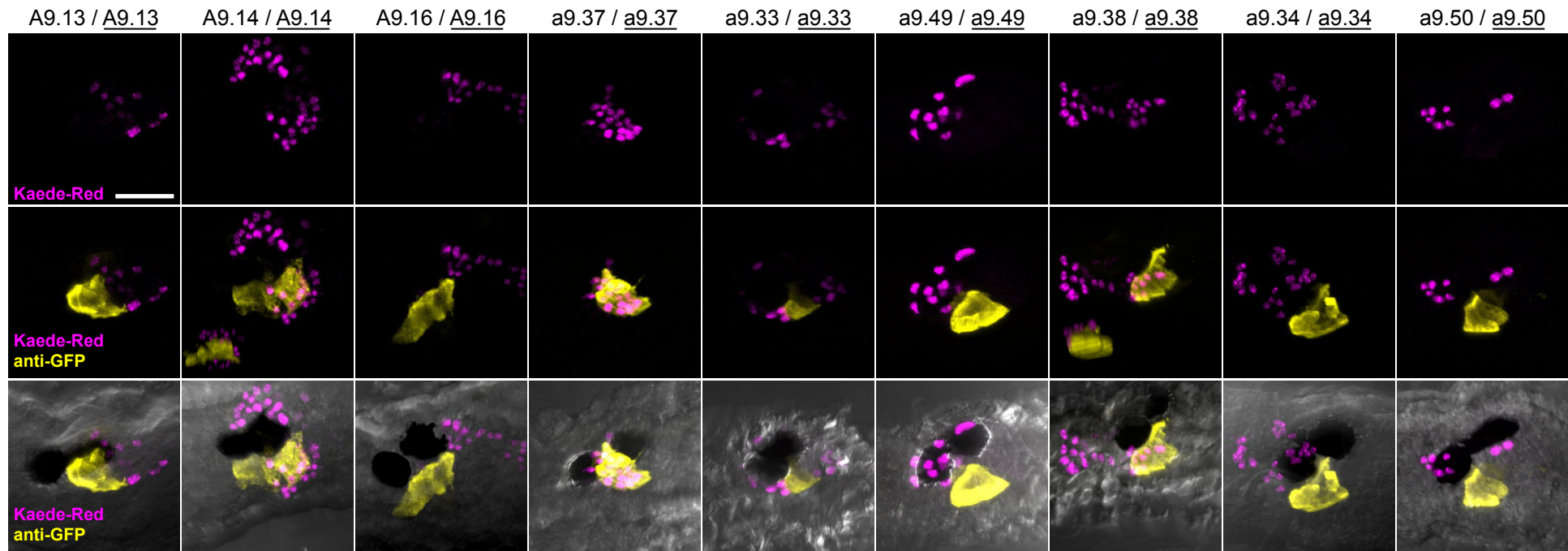


Fig. S1. Little position variation of cells labeled with the photo-converted Kaede among individuals. Other individuals with the larvae shown in Fig.1,2. Anterior is to the left. Lateral views. Scale bars: 10 μ m.

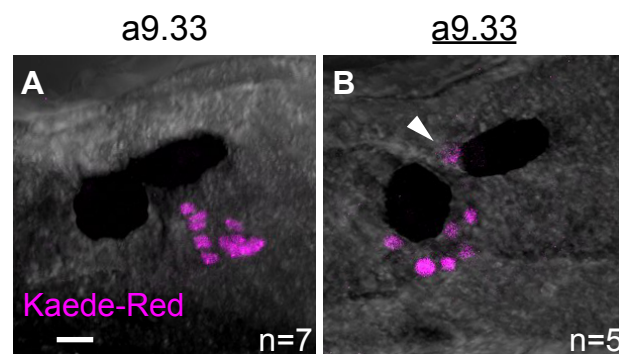


Fig. S2. Movement of a9.33/a9.33 cells through the embryogenesis. (A,B) Asymmetric distribution of descendants of left and right a9.33 cells. Anterior is to the left. Dorsal views. Nuclei of left (A) or right (B) a9.33-lineage cells were labeled by Kaede-red fluorescence (*magenta*). *White arrowhead*: A right a9.33-derived cell that did not move to the left side of the brain vesicle. Scale bars: 10 μ m.

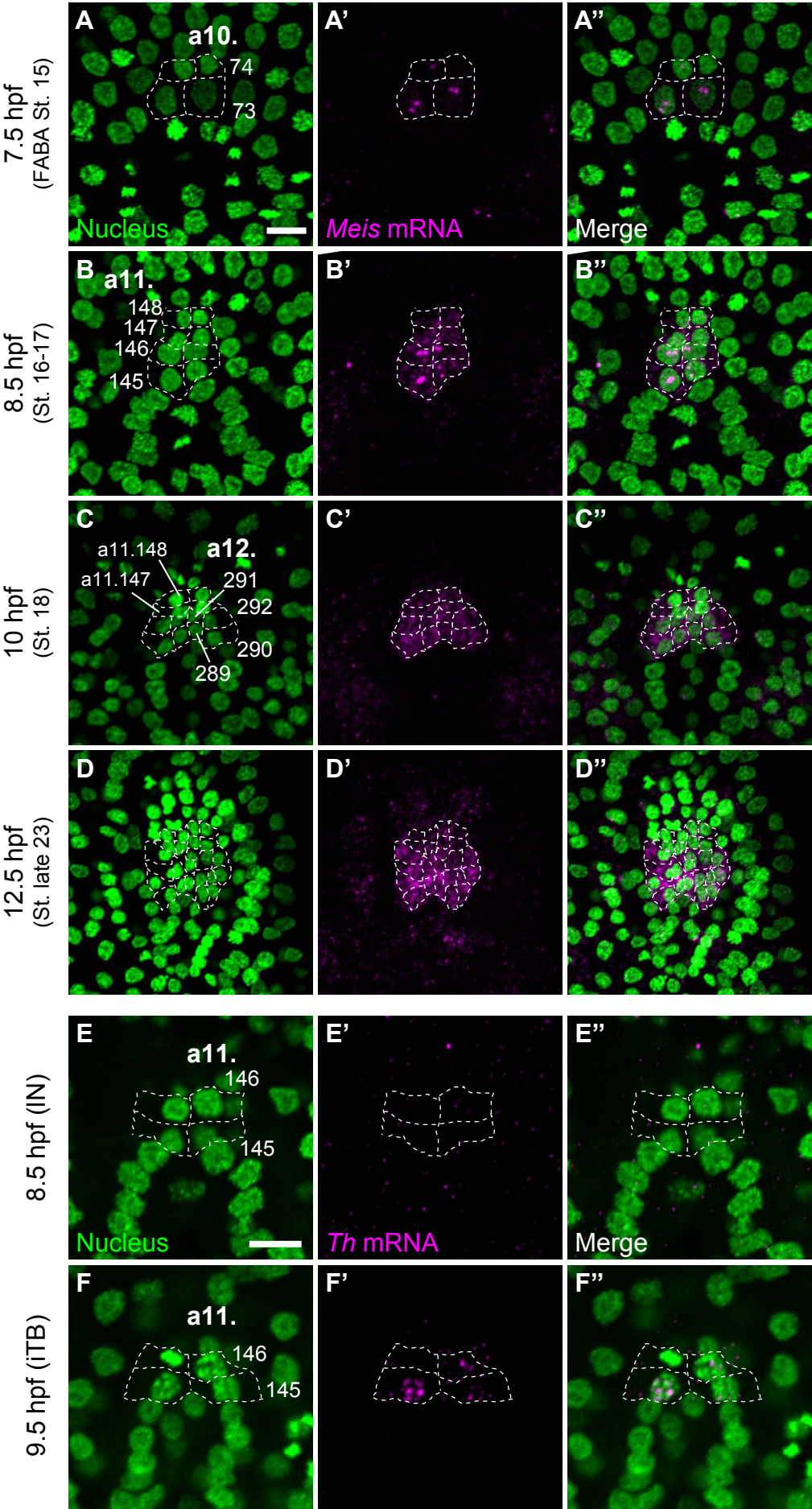


Fig. S3. Spatio-temporal expression patterns of *Meis* and *Th*. (A–F”) Anterior is to the top. Dorsal views. *Meis* mRNA (A–D”) and *Th* mRNA (E–F”) (*magenta*) were detected by WISH at the indicated stages (hpf and FABA stages). Nuclei were counter-stained with DAPI (*green*). *White dotted lines*: a9.37-lineage cells. iTB, initial tailbud; IN, late neurula. Scale bars: 10 μ m.

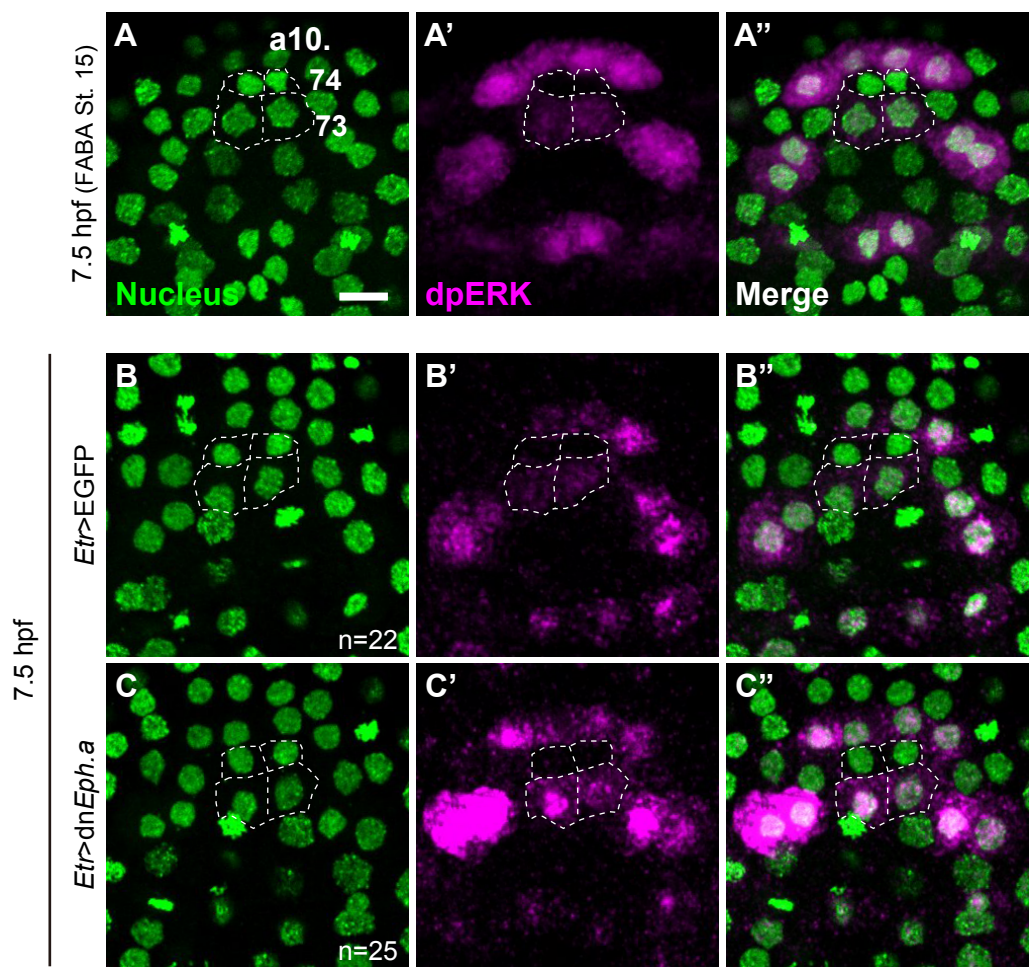


Fig. S4. Cells in which the MAPK pathway is activated in the neural plate and overexpression of the dominant negative form of *Eph.a* (dn*Eph.a*) receptor. (A–C'') The immunofluorescent staining of dpERK (magenta) at 7.5 hpf. Nuclei were counter-stained with DAPI (green). White dotted lines: The daughter cells of a9.37 cells. (B–C'') dpERK was not detected in a10.74 cells of the control embryos (B–B'') and the embryos overexpressing dnEph.a (C–C''). Anterior is to the top. Dorsal views. Scale bars: 10 μ m.

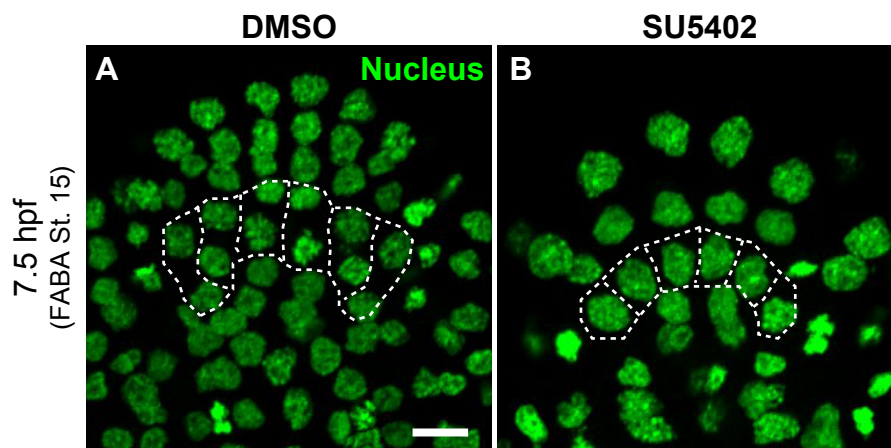


Fig. S5. Cells in row III of the neural plate do not divide by the treatment with SU5402. (A,B) Neurula embryos treated with DMSO (A) or an FGF receptor inhibitor, SU5402 (B). Anterior is to the top. Dorsal views. Nuclei were stained with DAPI (green). White dotted lines indicate cells in the row III of the neural plate including the a9.37-lineage cells. Scale bars: 10 μ m.

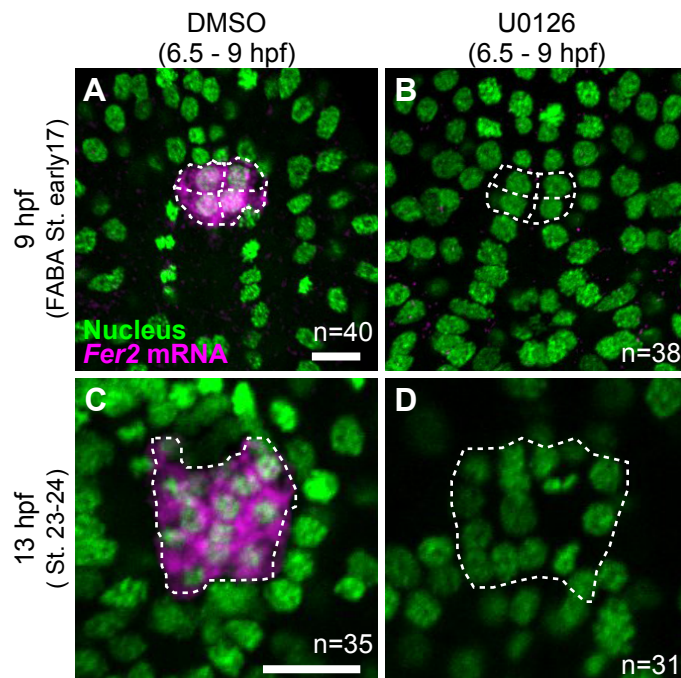


Fig. S6. MAPK pathway is required for the maintenance of *Fer2* expression after the neurula stage. (A–D) *Fer2* mRNA (magenta) was detected in embryos treated with DMSO (A,C) or U0126 (B,D) by the fluorescent-WISH. Green: Nuclei counter-stained with DAPI. Anterior is to the top. Dorsal views. White dotted lines: descendants of a10.73 cells. Scale bars: 10 μm.

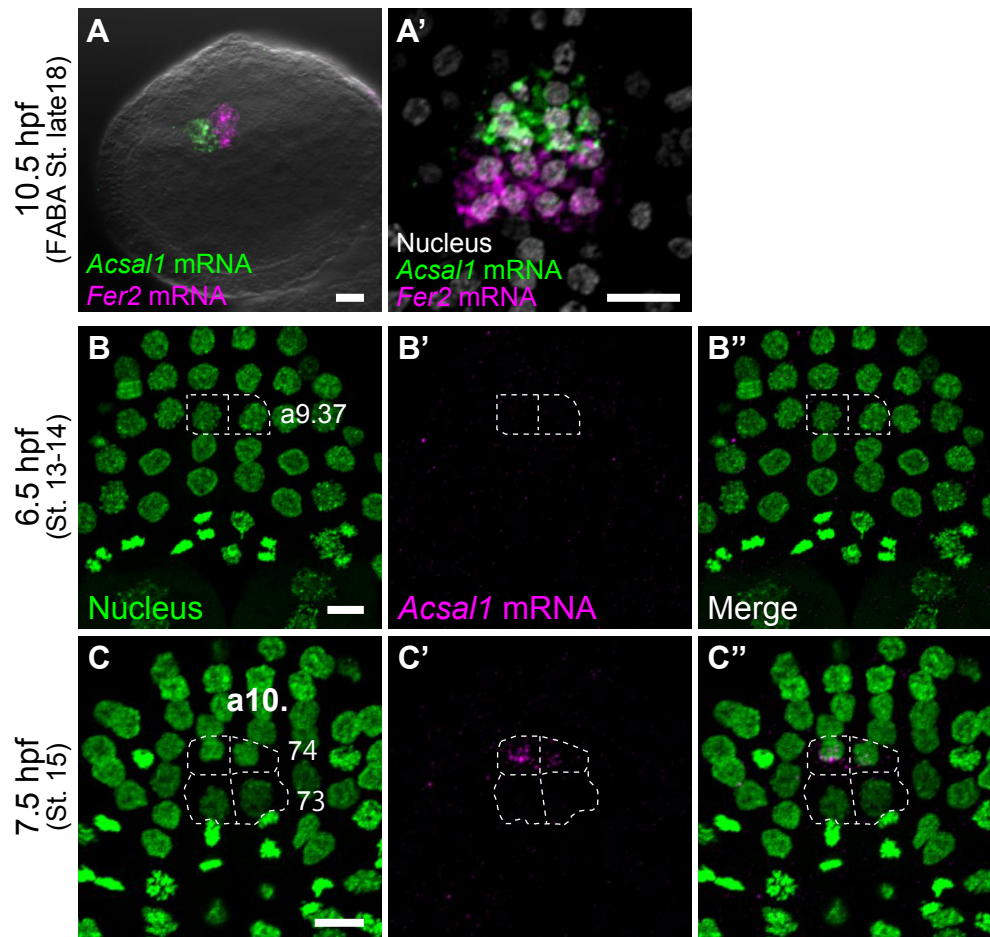


Fig. S7. The *Acsal1* gene is specifically expressed in the a10.74-lineage cells. (A,A') Comparison of expression patterns between *Acsal1* and *Fer2* genes at the early tailbud stage (10.5 hpf) by WISH. (A) Anterior is to the left. Lateral views. (A') Nuclei were counter-stained with DAPI (gray). Anterior is to the top. Dorsal views. (B–C'') *Acsal1* mRNA (magenta) was detected at 6.5 hpf (B–B'') and 7.5 hpf (C–C'') by fluorescent-WISH. Nuclei were counter-stained with DAPI (green). Anterior is to the top. Dorsal views. White dotted lines: a9.37 cells (B–B''), a10.73 and a10.74 cells (C–C''). Scale bars: 10 μ m.

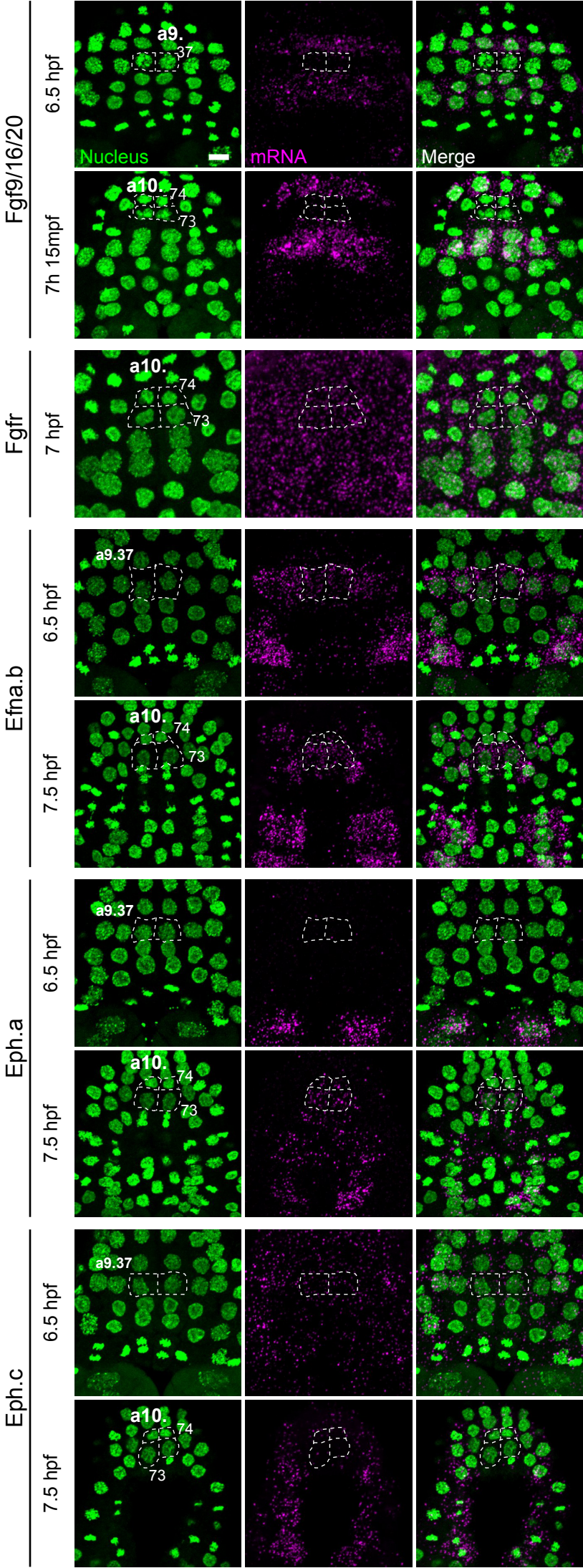


Fig. S8. The expression patterns of *Fgf9/16/20*, *Fgfr*, *Efna.b*, *Eph.a* and *Eph.c* before and after the a9.37 cell division. The expression of each gene was detected by WISH (*magenta*). Nuclei were counter-stained with DAPI (*green*). Anterior is to the top. Dorsal views. *White dotted lines*: a9.37-lineage cells. Scale bar: 10 μm .

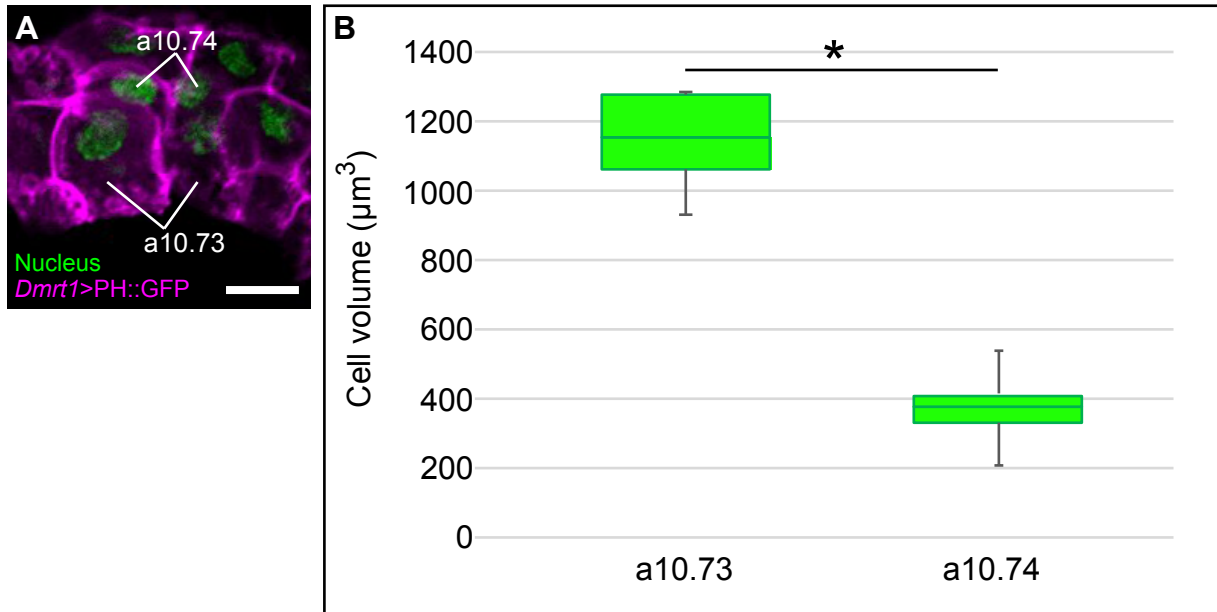


Fig. S9. The cell volume of a10.73 cells is higher than that of a10.74 cells. (A) The detection of membrane localized GFP (PH::GFP) expression (*magenta*) by the immunofluorescent staining against GFP. Nuclei were counter-stained with DAPI (*green*). Anterior is to the top. Dorsal views. (B) Boxplots indicate the cell volumes of a10.73 and a10.74 cells ($n=5$). The average volumes are $1120.52 \mu\text{m}^3$ (a10.73) and $361.376 \mu\text{m}^3$ (a10.74), respectively. Scale bar: $10 \mu\text{m}$. Statistical analysis was done by standard Student *t*-test. (* $P < 0.001$).

Table S1. The average number of cells expressing *Fer2* reporter at the larval stage

labeled cells†	Cells expressing <i>Fer2</i> reporter		n=
	only Kaede–Green positive	Kaede–Red positive	
Left a9.37	7.6 ± 0.40	8 ± 0.00	5
Right a9.37	7.25 ± 0.48	8 ± 0.00	4

†The cells labeled with Kaede red fluorescence at the late gastrula stage.

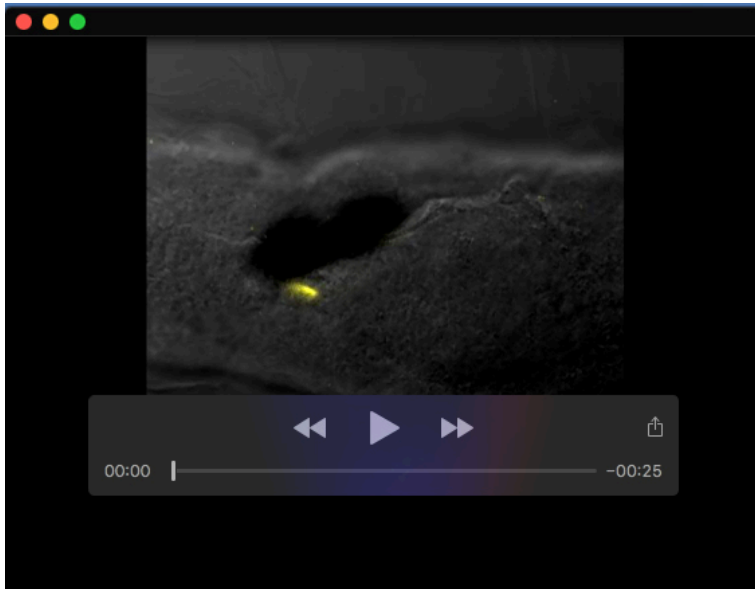
The numbers of cells are presented as mean ± standard error (s.e.m.).

Table S2. The average number of cells in the larval brain vesicle derived from each pair of neural plate cells

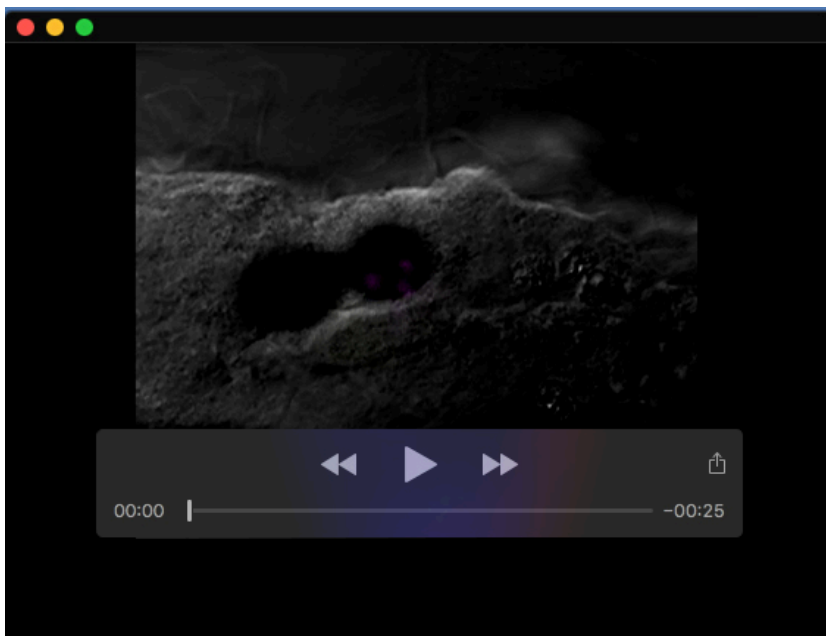
Labeled cells†	The average labeled cell number	s.e.m.	n=
a9.37/a9.37	23.5	0.50	4
a9.33/a9.33	17.7	0.95	6
a9.49/a9.49	9.5	0.29	4
a9.38/a9.38	23.6	0.24	5
a9.34/a9.34	24.3	0.25	4
a9.50/a9.50	12.2	1.36	5
A9.13/A913	24.8	0.77	6
A9.14/A914	48	1.22	5
A9.16/A916	48.3	1.11	4

†The cells labeled with red fluorescence of photo-converted Kaede at the late gastrula stage.

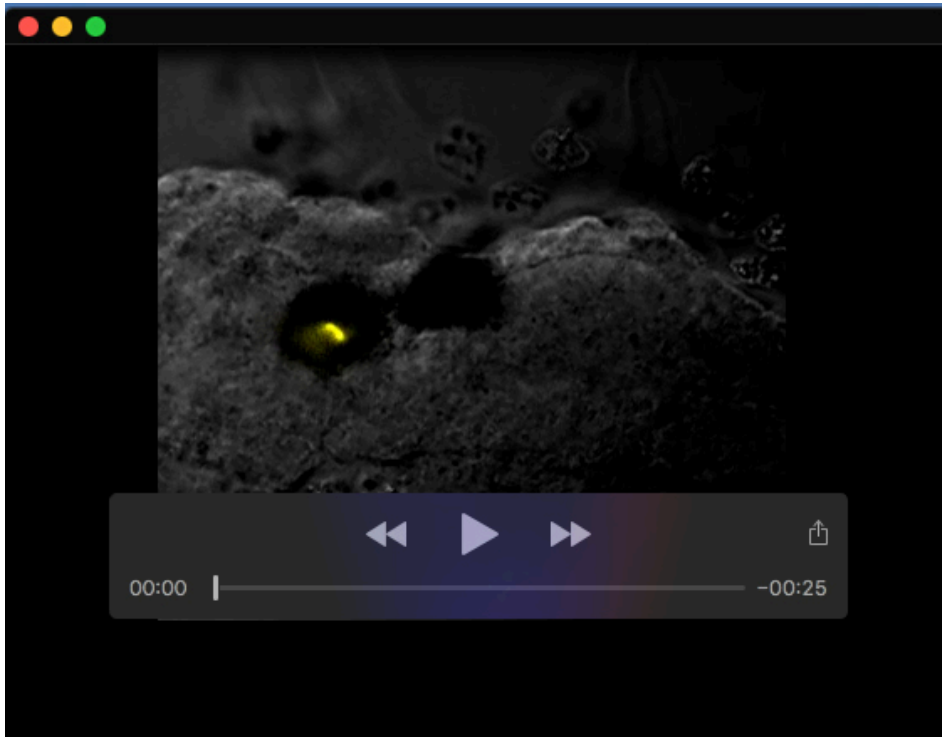
The cell numbers and standard error of the mean (s.e.m.) are shown.



Movie 1. Serial optical sections of confocal images of A9.13/A9.13 lineage-cells in the *Ciona* larva shown in Fig. 1E–E’. Localization of the fluorescence of Kaede-red and *Fer2*>EGFPv were visualized in magenta and yellow, respectively. Anterior is to the left. Lateral views. This movie progresses from dorsal to ventral regions of the larva.



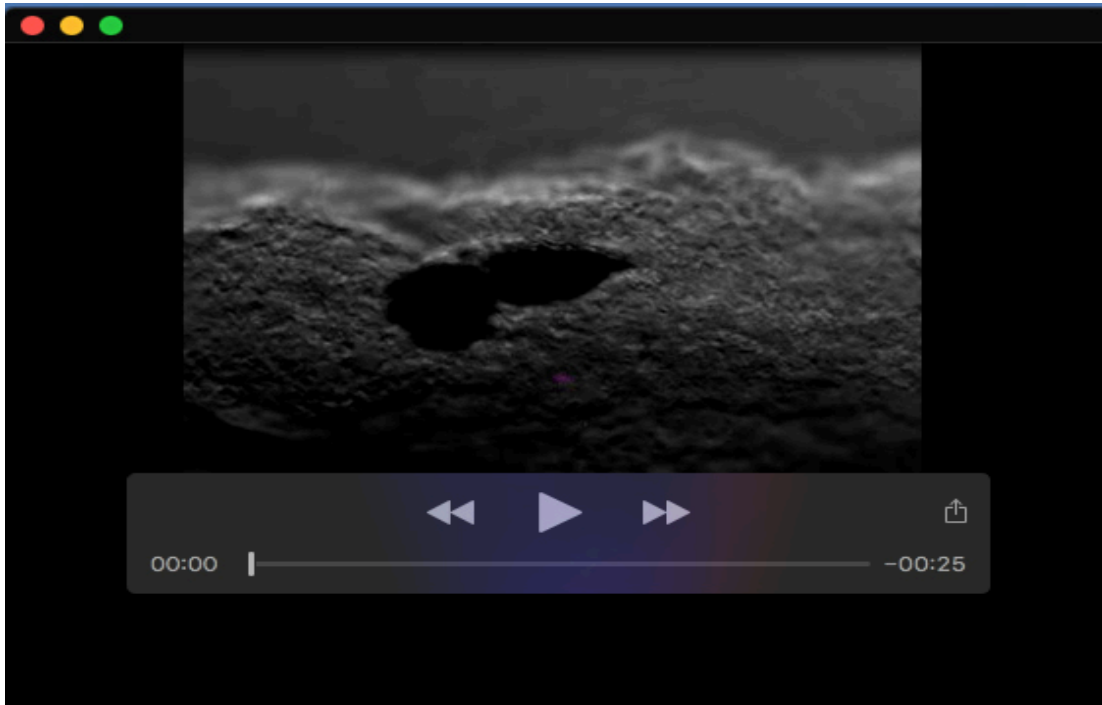
Movie 2. Serial optical sections of confocal images of A9.14/A9.14 lineage-cells in the *Ciona* larva shown in Fig. 1G–G’. Localization of the fluorescence of Kaede-red and *Fer2*>EGFPv were visualized in magenta and yellow, respectively. Anterior is to the left. Lateral views.



Movie 3. Serial optical sections of confocal images of A9.16/A9.16 lineage-cells in the *Ciona* larva shown in Fig. 1I–I’. Localization of the fluorescence of Kaede-red and *Fer2*>EGFPv were visualized in magenta and yellow, respectively. Anterior is to the left. Lateral views.



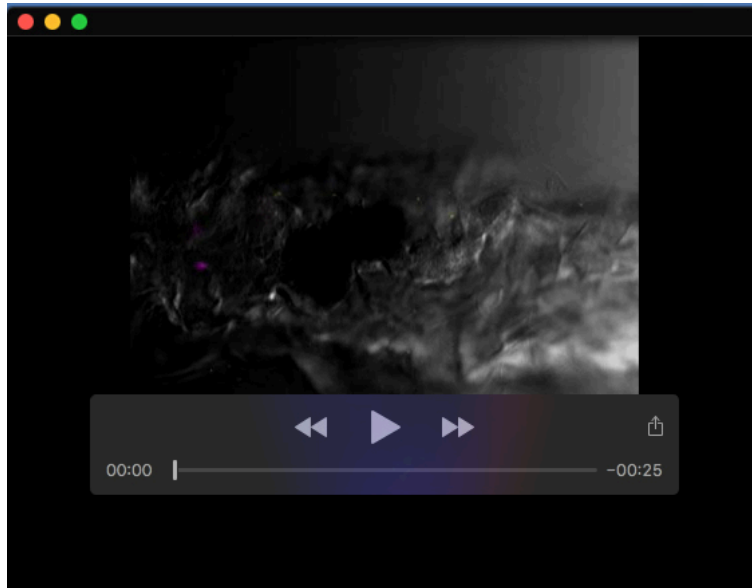
Movie 4. Serial optical sections of confocal images of a9.37/a9.37 lineage-cells in the *Ciona* larva shown in Fig. 2G–G’. Localization of the fluorescence of Kaede-red and *Fer2*>EGFPv were visualized in magenta and yellow, respectively. Anterior is to the left. Lateral views.



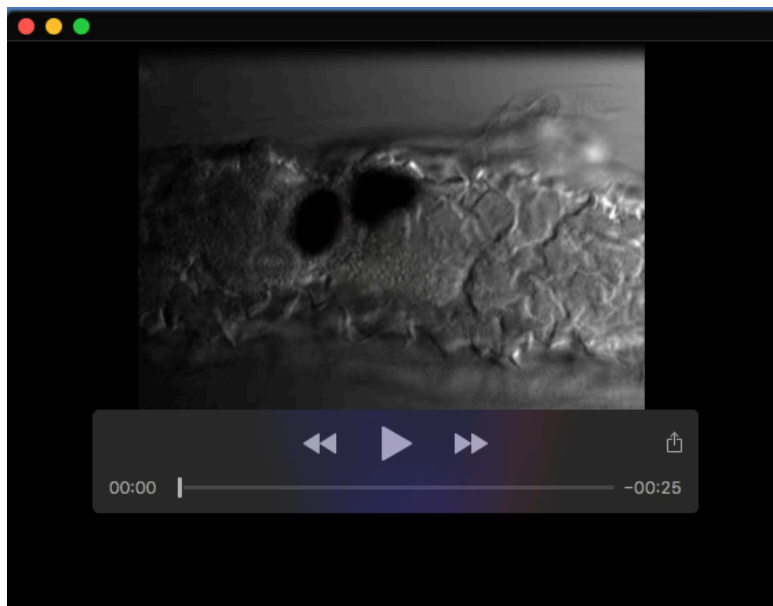
Movie 5. Serial optical sections of confocal images of a9.33/a9.33 lineage-cells in the *Ciona* larva shown in Fig. 2H–H’’. Localization of the fluorescence of Kaede-red and *Fer2*>EGFPv were visualized in magenta and yellow, respectively. Anterior is to the left. Lateral views.



Movie 6. Serial optical sections of confocal images of a9.49/a9.49 lineage-cells in the *Ciona* larva shown in Fig. 2I–I’’. Localization of the fluorescence of Kaede-red and *Fer2*>EGFPv were visualized in magenta and yellow, respectively. Anterior is to the left. Lateral views.



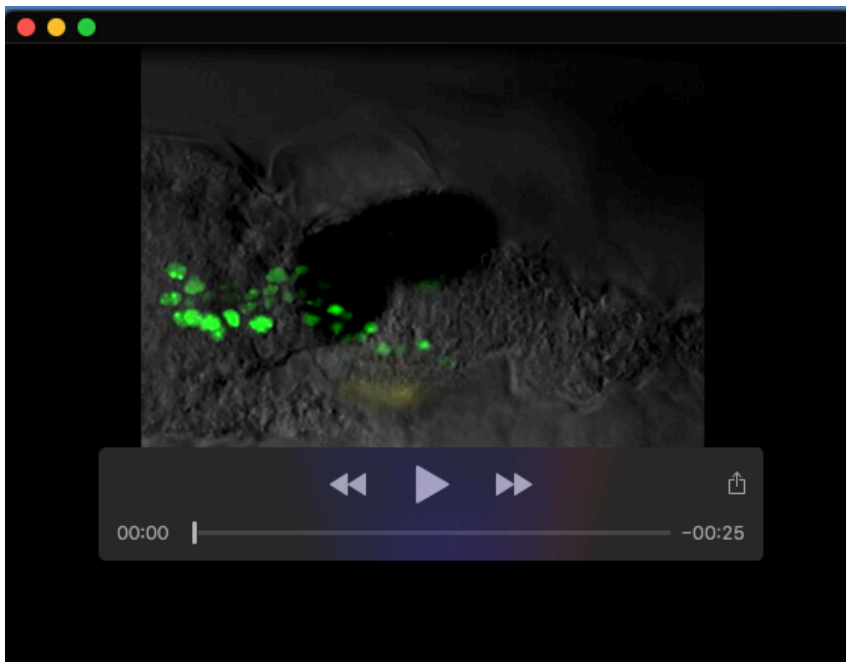
Movie 7. Serial optical sections of confocal images of a9.38/a9.38 lineage-cells in the *Ciona* larva shown in Fig. 2J–J’. Localization of the fluorescence of Kaede-red and *Fer2*>EGFPv were visualized in magenta and yellow, respectively. Anterior is to the left. Lateral views.



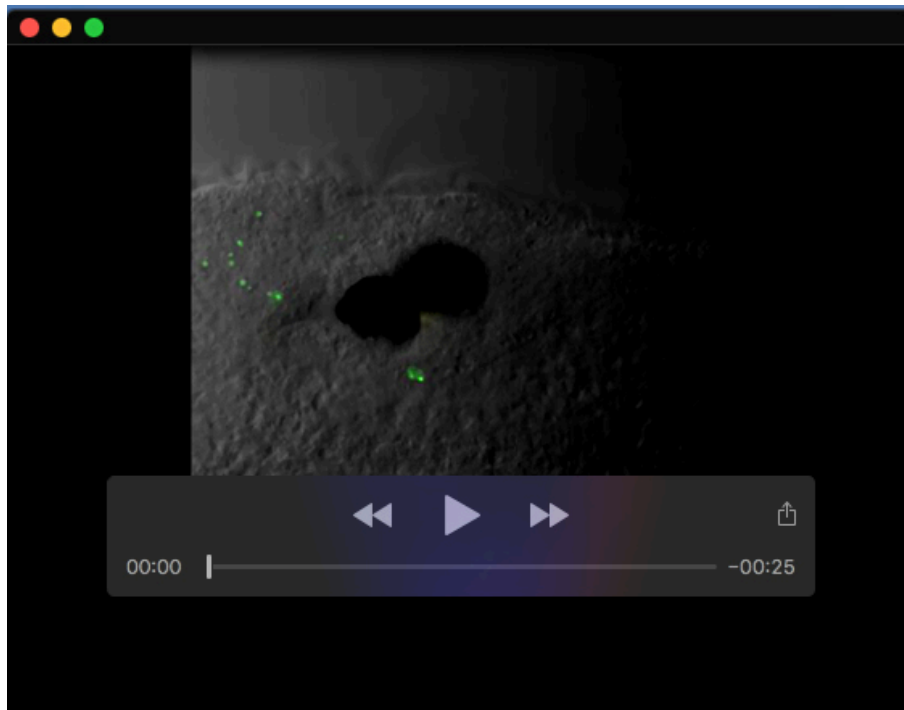
Movie 8. Serial optical sections of confocal images of a9.34/a9.34 lineage-cells in the *Ciona* larva shown in Fig. 2K–K’. Localization of the fluorescence of Kaede-red and *Fer2*>EGFPv were visualized in magenta and yellow, respectively. Anterior is to the left. Lateral views.



Movie 9. Serial optical sections of confocal images of a9.50/a9.50 lineage-cells in the *Ciona* larva shown in Fig. 2L–L’’. Localization of the fluorescence of Kaede-red and *Fer2*>EGFPv were visualized in magenta and yellow, respectively. Anterior is to the left. Lateral views.



Movie 10. Serial optical sections of confocal images of left a9.37 lineage-cells in the *Ciona* larva shown in Fig. 3B–B’’. Localization of the fluorescence of Kaede-green, Kaede-red and *Fer2*>EGFPv were visualized in green, magenta and yellow, respectively. Anterior is to the left. Lateral views.



Movie 11. Serial optical sections of confocal images of right a9.37 lineage-cells in the *Ciona* larva shown in Fig. 3D–D’’. Localization of the fluorescence of Kaede-green, Kaede-red and *Fer2*>EGFPv were visualized in green, magenta and yellow, respectively. Anterior is to the left. Lateral views.